FACULTY OF MECHANICAL ENGINEERING TUL

Master Thesis

Získávání energie z úplavu za válcem pomocí piezoelementů

Study programme: N0715A270018 Machines and Equipment Design
Author: **Mwikisa Mwikisa**
Thesis Supervisors: Ing. Shehab Ashraf Ahmed Salem, Ph.D.
Department of Power Engineering Equipment

Liberec 2024

Master Thesis Assignment Form

Získávání energie z úplavu za válcem pomocí piezoelementů

Name and surname:	**Mwikisa Mwikisa**
Identification number:	S22000180
Study programme:	N0715A270018 Machines and Equipment Design
Assigning department:	Department of Power Engineering Equipment
Academic year:	2023/2024

Rules for Elaboration:

Smart Materials are the materials whose physical or chemical native properties can be significantly changed when subjected to changes in their environment. Their unique abilities allow their use in various applications involving the harvesting of ambient energy in the environment. The ability of Piezoelectric materials to change between electric and pressure energies and vice-versa has rendered them as a favorable option for harvesting of vibrational energy.
Various piezoelectric transducer designs have been implemented to harvest the energy of flow-induced vibrations, where a piezoelectric transducer is either immersed in a fluid or attached to a body that is in the fluid, and hence harvests its vibrations' energy.
This work shall look at new possibilities for energy harvesting that is based on vortex-shedding off cylinders immersed across airflow. The subject of this diploma thesis is the design of a harvester of flow-induced vibrations, which uses piezoelectric elementsfor transduction. The main goal is the analysis of flow fields around the body undergoing the vibration. For the investigation, the use of either of CFD methods using Ansys Fluent or suitable experiments is assumed.
Work plan:

- Review of the literature on Flow-induced Vibration Harvesting, applications, of piezoelectricity, and CFD.
- Study of suitable CFD models to model the problem considering Fluid Structure Interaciton.
- Design of the Experiment.
- Performing anlysis at various airpseeds and turbulence conditions.
- Results assesment and discussion..

Scope of Graphic Work:	5 p.
Scope of Report:	50 p.
Thesis Form:	printed/electronic
Thesis Language:	english

List of Specialised Literature:

1. SALEM, Shehab and FRAŇA, Karel. A Wind Tunnel Study of the Flow-Induced Vibrations of a Cylindrical Piezoelectric Transducer. *Sensors*. 2 May 2022. Vol. 22, no. 9, p. 3463. DOI 10.3390/s22093463..
2. ZDRAVKOVICH, M. M. *Flow around circular cylinders. 1.* . Reprint. Oxford : Oxford University Press, 2007. ISBN 978-0-19-856396-9.
3. YANG, Jiashi. An introduction to the theory of piezoelectricity. Advances in mechanics and mathematics, vol. 9. New York: Springer, 2005. ISBN 0-387-23573-6.

Thesis Supervisors:	Ing. Shehab Ashraf Ahmed Salem, Ph.D. Department of Power Engineering Equipment
Date of Thesis Assignment:	November 1, 2023
Date of Thesis Submission:	April 30, 2025

L.S.

doc. Ing. Jaromír Moravec, Ph.D.
Dean

doc. Ing. Martin Bílek, Ph.D.
study programme guarantor

Liberec November 1, 2023

Declaration

I hereby certify, I, myself, have written my master thesis as an original and primary work using the literature listed below and consulting it with my thesis supervisor and my thesis counsellor.

I acknowledge that my master thesis is fully governed by Act No. 121/2000 Coll., the Copyright Act, in particular Article 60 – School Work.

I acknowledge that the Technical University of Liberec does not infringe my copyrights by using my master thesis for internal purposes of the Technical University of Liberec.

I am aware of my obligation to inform the Technical University of Liberec on having used or granted license to use the results of my master thesis; in such a case the Technical University of Liberec may require reimbursement of the costs incurred for creating the result up to their actual amount.

At the same time, I honestly declare that the text of the printed version of my master thesis is identical with the text of the electronic version uploaded into the IS/STAG.

I acknowledge that the Technical University of Liberec will make my master thesis public in accordance with paragraph 47b of Act No. 111/1998 Coll., on Higher Education Institutions and on Amendment to Other Acts (the Higher Education Act), as amended.

I am aware of the consequences which may under the Higher Education Act result from a breach of this declaration.

May 10, 2024 Mwikisa Mwikisa

Abstrakt

Tato práce zkoumá možnosti získávání energie z vibrací vyvolaných prouděním pomocí piezoelektrického válce vystaveného proudění vzduchu. Experimentální zařízení, navržené pro optimalizaci zachycování energie, obsahuje piezoelektrický prvek vyrobený z PZT-5A, podpůrné konstrukce, zdroj proudění vzduchu a sofistikované vybavení pro sběr dat.

Studie začíná podrobnou analýzou charakteristik proudění vzduchu, určením potřebné doby vzorkování a zmapováním profilu rychlosti na různých místech, aby se určila optimální poloha piezoelektrického válce. Zjištění naznačují, že umístění válce 8 cm od výstupu použitého axiálního ventilátoru poskytuje nejrovnoměrnější proudění vzduchu, což je nezbytné pro maximalizaci vibrační odezvy a účinnosti získávání energie.

Měření piezoelektrického napětí prokazují jasný vztah mezi rychlostí proudění vzduchu, nastavením ventilu a generovaným RMS napětím. Vyšší rychlosti vzduchu korelují se zvýšenými výstupy RMS napětí, zejména při optimálním nastavení výstupních ventilů, což potvrzuje potenciál pro přesné vyladění systému pro maximalizaci využití energie.

Abstract

This thesis investigates the potential of harvesting energy from flow-induced vibrations using a piezoelectric cylinder subjected to airflow. The experimental setup, designed to optimise energy capture, comprises a piezoelectric element made from PZT-5A, support structures, an airflow source, and sophisticated instrumentation for data acquisition.

The study begins with a detailed analysis of the airflow characteristics, determining the necessary sampling time and mapping the speed profile at various locations to identify the optimal position for the piezoelectric cylinder. Findings indicate that positioning the cylinder 8 cm from the outlet of the axial ventilator used provides the most uniform airflow, essential for maximising vibrational response and energy harvesting efficiency.

Piezoelectric voltage measurements demonstrate a clear relationship between airflow speed, valve settings, and generated RMS voltage. Higher air speeds correlate with increased RMS voltage outputs, particularly at the optimal outlet valve settings, confirming the potential for precise system tuning to maximise energy harvesting.

Contents

List of Figures

List of Tables

List of Symbols

ρ (rho) ---------- Fluid density

u----------Characteristic flow velocity (also used as free-stream velocity)

L----------Characteristic length scale (e.g., the width of an object)

μ (mu) ----------Dynamic viscosity of the fluid

Re----------Reynolds number

St----------Strouhal number

f----------Frequency of vortex shedding

D----------Cylinder diameter

d coefficients----------Electric displacement generated per unit mechanical stress

g coefficients----------Electric field generated per unit mechanical strain

e coefficients----------Electric field generated per unit mechanical stress

h coefficients----------Magnetic field generated per unit mechanical strain

ϵ (epsilon) ----------Dielectric constant

tan δ (delta) ----------Dielectric loss

Tc----------Curie temperature

Qm----------Mechanical quality factor

PZT----------Lead Zirconate Titanate

FIV----------Flow-Induced Vibrations

1. Introduction

Since the dawn of civilization, energy in various forms has played an integral role in societal development. In recent decades, the urgency of sustainability has taken centre stage, driven by concerns over climate change and the depletion of fossil fuel reserves. This shift has spurred a growing interest in renewable energy sources, such as wind, solar, tidal, and hydroelectric power. Amid these advancements, the conversion of flow-induced mechanical energy into electrical power emerges as an innovative and promising field.

This master's thesis embarks on an exploration of this fascinating domain, with a specific focus on the utilisation of piezoelectric elements to harvest energy from flow-induced vibrations behind a cylinder. Piezoelectric materials, known for their remarkable ability to convert mechanical strain into electrical energy, offer a unique and efficient approach to energy harvesting. The phenomenon of flow-induced vibrations, which occurs when fluid flows around a bluff body like a cylinder, presents a valuable opportunity to harness mechanical energy.

By investigating the dynamics of flow-induced vibrations and optimising the piezoelectric energy conversion process, this research aims to develop sustainable energy solutions that harness the ubiquitous and often untapped mechanical energy present in fluid flows. This study not only contributes to the growing body of knowledge in renewable energy technologies but also has the potential to inspire innovative applications in various engineering fields. Through this work, we strive to advance the understanding and practical implementation of piezoelectric energy harvesting, paving the way for more sustainable and efficient energy systems.

1.1. Smart Materials and piezoelectricity

Smart materials, also known as intelligent or responsive materials, constitute a fascinating class of materials. These materials exhibit the remarkable ability to alter their properties in response to external stimuli. Whether it's temperature fluctuations, changes in light intensity, variations in pressure, or the influence of magnetic fields, smart materials swiftly sense and adapt to optimise their performance [1].

1.1.1. Types of Smart Materials

Below are various types of smart materials:

1. Shape Memory Alloys: Shape memory alloys possess a unique memory—they can remember and return to their original shape when subjected to specific stimuli, such as heat. These materials find applications in medical devices, aerospace components, and consumer products [2].
2. Piezoelectric Materials: Piezoelectric materials generate an electrical charge when mechanical stress or pressure is applied to them. These remarkable materials play crucial roles in sensors, actuators, energy harvesting devices, and even everyday items like lighters [3].
3. Electroactive Polymers: Electroactive polymers change shape or size when an electric field is applied. This property is harnessed in robotics and artificial muscles, making them essential for various applications [4].
4. Thermochromic Materials: Thermochromic materials undergo reversible colour changes in response to temperature variations. These materials are commonly used in smart windows, textiles, and temperature-sensitive labels [5].

1.1.2. Piezoelectricity

Piezoelectricity is a fascinating phenomenon exhibited by specific materials. When these materials are deformed or compressed, the arrangement of their atoms or molecules changes. As a result, positive and negative charges separate within the material, creating an electric potential difference or voltage. Conversely, when an electric field is applied, the material deforms due to the movement of charges [4].

Piezoelectric elements are transducers with the unique ability to generate electric charges when exposed to mechanical stress or deformation, as is the case with flow-induced vibrations. Their capacity to convert between electric and pressure energies has made them a favourable choice for harvesting vibrational energy. Studies have shown that piezoelectric materials such as Lead Zirconate Titanate (PZT) exhibit high energy conversion efficiency when subjected to flow-induced vibrations [6]. Optimising the positioning and orientation of piezoelectric elements within the wake of a cylinder significantly enhances energy conversion efficiency and, therefore, by strategically positioning piezoelectric elements in the wake of the cylinder, we can capture and harness energy from the flow to generate electricity.

Examples of Piezoelectric Materials

Some notable piezoelectric materials include:

- **Quartz**: This crystalline form of silicon dioxide (SiO_2) finds applications in electronic devices, including watches, sensors, and resonators [3].
- **Lead Zirconate Titanate (PZT)**: A ceramic composite of Lead Zirconate ($PbZrO_3$) and Lead Titanate ($PbTiO_3$), PZT is extensively used in actuators, sensors, and transducers due to its exceptional properties [3].
- **Polyvinylidene Fluoride (PVDF)**: A flexible and lightweight polymer, PVDF is versatile in shaping and molding. It is employed in sensors, energy harvesting devices, and biomedical tools [3].
- **Gallium Orthophosphate ($GaPO_4$)**: With exceptional properties suitable for high-temperature environments, $GaPO_4$ is used in sensors and actuators designed for harsh conditions [3].
- **Lithium Niobate ($LiNbO_3$)**: A nonlinear ferroelectric material, $LiNbO_3$ is extensively utilized in optoelectronics and surface acoustic wave devices. Its robust piezoelectric traits make it indispensable in telecommunications and optical devices [3].

Piezoelectric Properties

Piezoelectric materials, which convert mechanical stress into electrical charge and vice versa, are integral to numerous technological applications, such as sensors, actuators, and medical devices. The following key properties define their functionality:

1. **Piezoelectric Coefficients**

These coefficients play a crucial role in piezoelectric materials. Let's break them down:

- d coefficients: These describe the electric displacement generated per unit mechanical stress. For example, d_{33} represents the electric displacement along the third crystallographic axis when mechanical stress is applied [3].
- g coefficients: These describe the electric field generated per unit mechanical strain. For instance, g_{33} represents the electric field produced when the material experiences mechanical strain along the third axis [3].
- e and h coefficients: These coefficients serve similar functions but with alternate stress/strain and electrical units. They are essential for understanding the material's behaviour during mechanical-to-electrical energy conversion [3].

2. **Dielectric Properties**

Dielectric properties are critical for energy storage applications:

- Dielectric constant (ϵ): This measures how much charge a material can store at a given electric field. High dielectric constants are desirable for capacitors, where charge storage capacity matters [3].
- Dielectric loss (tan δ): This quantifies energy dissipation due to dielectric losses. Lower tan δ values indicate better energy storage efficiency [3].

3. **Curie Temperature (Tc)**

The Curie temperature is the point at which a piezoelectric material loses its piezoelectric properties due to a phase transition. Above this temperature, the crystalline structure becomes symmetric, disrupting the non-centrosymmetric alignment necessary for piezoelectricity. Knowing the Curie temperature helps define the operational temperature range of piezoelectric devices [3].

4. **Temperature Stability**

   A material's temperature stability determines whether it can maintain its piezoelectric and dielectric properties across varying environmental conditions. Good temperature stability is essential for reliable performance in different temperature ranges [3].

5. **Mechanical Quality Factor (Qm)**

   The Qm factor reflects energy dissipation within a piezoelectric material during oscillation cycles. A higher Qm indicates lower energy loss. Materials with high Qm values are ideal for resonant applications like filters and oscillators [3].

Smart materials, with their adaptability and responsiveness to external stimuli, herald a new era in material science, enabling advancements across various sectors, including energy harvesting. Piezoelectric materials offer a promising avenue for converting mechanical energy from flow-induced vibrations into electrical energy. This energy harvesting technique not only showcases the innovative application of smart materials but also contributes to the sustainable energy solutions of the future. The versatility and efficiency of piezoelectric materials in energy conversion processes underscore their pivotal role in addressing the energy challenges of the modern world.

1.2. Fluid mechanics Introduction

Fluid mechanics is a vital area of engineering that studies the behaviour of fluids and their interactions with solid objects. This section introduces vortex shedding, a phenomenon characterised by the periodic formation and shedding of vortices behind objects like cylinders at certain velocities. It also provides an overview of flow-induced vibrations and examines critical dimensionless numbers, such as the Reynolds and Strouhal numbers, which are essential for understanding fluid dynamics in various engineering applications.

1.2.1. Vortex Shedding

Vortex shedding is a phenomenon that occurs when there is periodic formation and shedding of vortices in the wake of an object, such as a cylinder, at certain velocities [7].

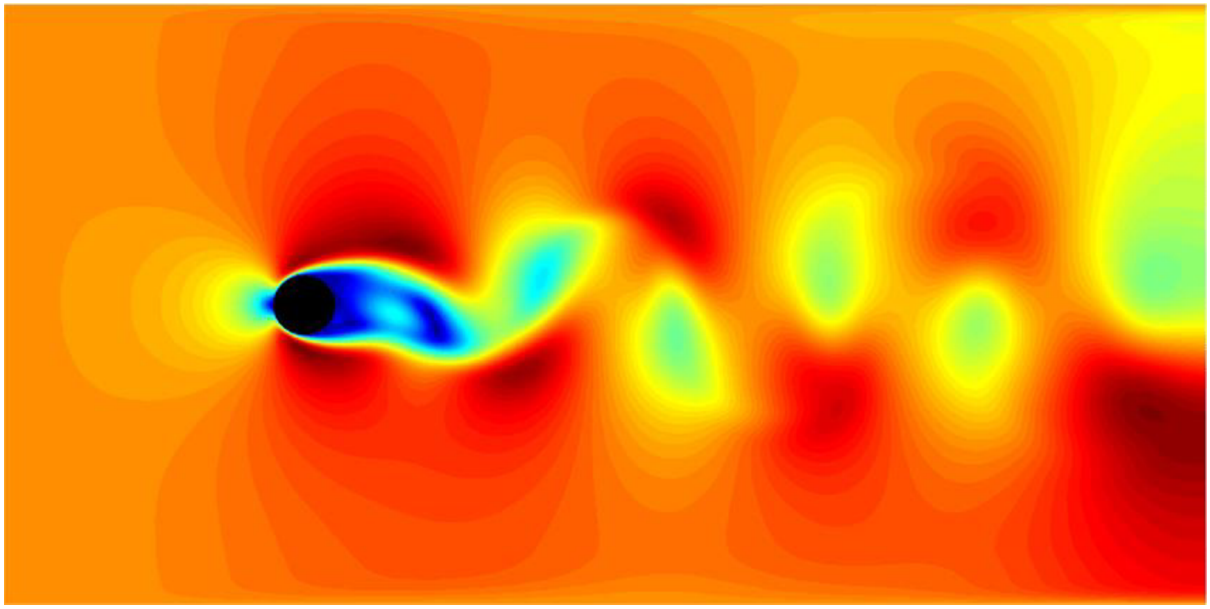

Figure 1 Vortex shedding in graphene at Reynolds number Re = 100, using a grid of 1024 × 512 cells [8]

Flow Around a Cylinder

The characteristics of flow around a cylinder evolve in response to fluctuations in the Reynolds number. With a gradual increase in the Reynolds number until reaching the critical point of vortex shedding, a series of changes occur, influencing the flow dynamics and introducing notable transformations [9].

Vortex Shedding Governing Equations

In the field of engineering, a comprehensive understanding of a physical phenomenon is often achieved by exploring the governing equations that describe its behavior. When studying vortex shedding, the significance of these equations becomes particularly pronounced. In the realms of aerodynamics and fluid dynamics, the study of vortex shedding plays a pivotal role. To grasp this phenomenon adequately, one must become familiar with the following equations:

• **Navier-Stokes Equations**: This equation is expressed in the x, y, and z directions, which represent the three spatial dimensions. It encompasses conservation of mass and momentum for a fluid [10].

$$\rho(\partial t \partial u + u \cdot \nabla u) = -\nabla p + \nabla \cdot \tau + \rho g$$

• **Momentum equation**: relates the sum of the forces acting on an element of fluid to its acceleration or rate of change of momentum [11].

$$\rho \frac{\partial v}{\partial t} = -\nabla p + \mu \nabla^2 v + F$$

• **Continuity equation**: This equation represents the conservation of mass, illustrating that the rate of change of mass within a control volume is zero [11].

$$\rho \frac{\partial v}{\partial t} + \nabla . \rho u = 0$$

• **Reynolds Number**: The Reynolds number, which compares inertial forces to viscous forces, is another crucial dimensionless parameter. It plays a critical role in understanding vortex shedding [12].

$$Re = \frac{\rho u L}{\mu}$$

Where:

Re = Reynolds number, ρ = Fluid density, u = Characteristic flow velocity, L = Characteristic length scale (e.g., the width of an object) and μ = Dynamic viscosity of the fluid

• **Strouhal Number (St)**: The Strouhal number (St) represents a dimensionless proportionality constant that relates the main frequency of vortex shedding to the free stream velocity divided by the dimensions of a bluff body. It is commonly approximated as a constant value. The dimensionless Strouhal number describes the relationship between the vortex shedding frequency and fluid velocity, and it can be expressed as: [13].

$$St = \frac{fL}{u}$$

Where:

St = Strouhal number, f = Frequency of vortex shedding, L = Characteristic length scale, u = Flow velocity

Factors Affecting Vortex Shedding

Several factors affect vortex shedding, including the shape and size of the object, the velocity and density of the fluid, and the flow conditions [7].

Applications of Knowledge of Vortex Shedding

Knowledge of vortex shedding has numerous applications:

• **Aerospace industry**: Designing efficient aircraft and wind turbines [9].

• **Civil engineering**: Designing bridges and tall buildings to withstand wind-induced vortex shedding forces [7].

• **Energy industry**: Harnessing energy from flow-induced vibrations, which is still in development [9].

Modes of Vortex Shedding

There are three modes of vortex shedding:

• **2S Mode (Symmetric)**: Characterized by a regular and symmetric shedding pattern, resulting in relatively stable flow [11].

• **2P Mode (Periodic)**: Shedding occurs alternately from both sides of the object at irregular intervals, typically observed at higher flow velocities [11].

• **3S Mode (Symmetric with Triple Formation)**: Vortices shed in groups of three from both sides of the object at regular intervals, observed at relatively high flow velocities [11].

Vortex shedding can pose challenges to structures, but understanding this phenomenon can help design safer and more efficient structures. Moreover, the potential of harnessing energy from

flow-induced vibrations underscores the importance of adequate knowledge of vortex shedding [9].

1.2.2. Understanding the Dynamics of Strouhal and Reynolds Numbers in Fluid Mechanics

The Strouhal number (St) and Reynolds number (Re) are important parameters in fluid mechanics, characterising flow regimes and dynamics behind bluff bodies [14]. The Strouhal number primarily describes the oscillating flow mechanisms and vortex shedding frequency, which are crucial for predicting flow-induced vibrations in engineering structures [15]. Meanwhile, the Reynolds number, essentially the ratio of inertial forces to viscous forces, defines distinct flow regimes spanning from laminar to turbulent. [12].

Understanding the interplay between these parameters enhances our ability to predict fluid behaviour and design structures that can withstand flow-induced stresses, ensuring safety and efficiency in engineering applications. [16].

Models of Strouhal Number

The theoretical model involving a cylinder in crossflow provides a mathematical framework to estimate the Strouhal number based on Reynolds number and shedding frequency [17]. The relationship is typically formulated as:

$$St = \frac{fD}{u}$$

Where f is the shedding frequency, D is the cylinder diameter, and u is the free-stream velocity. This model looks at vortex shedding dynamics induced by the fluid flow around the cylinder, considering the effects of fluid velocity and object dimensions [13].

Experimental Model: Von Kármán Vortex Street

The experimental approach involves direct observations of vortex shedding in laboratory settings or scaled models in wind tunnels. By placing a bluff body such as a cylinder in fluid flow and measuring the vortex shedding frequency and body dimensions, researchers determine the Strouhal number empirically [18]. This methodology validates and supports theoretical models and provides baseline data for empirical correlations.

Empirical Models for Various Bluff Bodies

Empirical models utilise extensive experimental data to estimate the Strouhal number under varying flow conditions and bluff body shapes. These models incorporate adjustments for body shape, Reynolds number, and specific flow scenarios, offering a pragmatic estimation method tailored to different bluff body configurations like aerofoils and square cylinders [19].

Dynamics of the Wake Strouhal Number

The Wake Strouhal number is significant in characterizing the wake structure and its effect on flow-induced vibrations [10]. It is particularly influenced by the distance from the object, which impacts wake dynamics and vortex shedding frequency. Understanding these relationships is vital for predicting flow behaviours and developing strategies to mitigate adverse effects on engineered structures.

Relationship Between Reynolds Number and Strouhal Number

When examining the connection between Reynolds number and Strouhal number across various Reynolds number regimes, we observe a transition from linear to nonlinear behaviour. This progression ultimately leads to asymptotic behaviour at high Reynolds numbers.

Linear Relationship: At low Reynolds numbers (Re < 2000), the relationship between Reynolds number and Strouhal number is described by $St=\alpha Re$.

St=αRe is typically linear, indicating straightforward dynamics generally found in laminar flow regimes [14].

Nonlinear Relationship: As Reynolds number increases (2000 < Re < 10,000), the relationship becomes nonlinear, described by:

$St=\beta Re\gamma$

This reflects the onset of transitional flows [17].

Asymptotic Behaviour: At very high Reynolds numbers (Re > 10,000), the Strouhal number approaches an asymptotic value. The relationship is described by:

$St = St_{\infty}$

This illustrates minimal changes despite increasing Reynolds number, a characteristic of fully developed turbulent flows [16].

A deep understanding of the Strouhal and Reynolds numbers, along with their intricate connections, is pivotal in the fields of fluid dynamics and engineering. By analysing these relationships from theoretical, experimental, and empirical perspectives, we acquire valuable insights that fuel innovations in system design and operation for applications exposed to fluid flows. This knowledge is essential for improving safety, optimising performance, and ensuring reliability across diverse engineering disciplines.

1.3. Flow-Induced Vibrations and their types

Flow-induced vibrations (FIV) are a complex phenomenon resulting from the interaction between fluid flow and structures [20]. These vibrations are widespread, impacting various engineered systems such as bridges, pipelines, aircraft, and even musical instruments [21]. The essence of FIV lies in the oscillatory motions triggered by the dynamic interaction between an object and the surrounding fluid. This section investigates the fundamental principles of flow-induced vibrations, exploring their classification, underlying mechanisms, and the factors influencing their occurrence. Understanding FIV is crucial not only for mitigating their potential effects on structural integrity and longevity but also for exploring innovative approaches to energy harvesting, particularly using piezoelectric elements to capture energy from flow-induced oscillations [21].

1.3.1. Classification of Flow-Induced Vibrations

Flow-induced vibrations (FIV) are categorized based on the nature of the interaction between the fluid flow and the object [20]. This section outlines the primary types of FIV, namely vortex shedding-induced vibrations, galloping, flutter, and turbulence-induced vibrations. Each category exhibits unique characteristics and underlying mechanisms, necessitating distinct approaches for analysis, mitigation, and energy harvesting [21].

Vortex Shedding-Induced Vibrations

Figure 2 illustrates the phenomenon of vortex shedding around a cylinder exposed to wind flow.

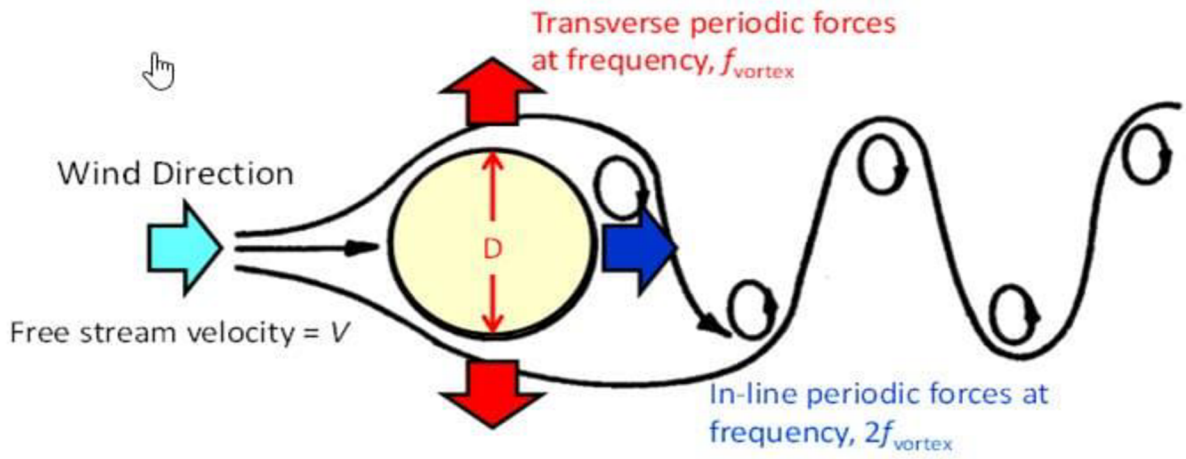

Figure 2 Vortex Shedding-Induced Vibrations [15]

Galloping

Galloping, also known as aeroelastic galloping, is characterized by large-scale, low-frequency motions of slender structures subjected to crossflow [20]. While this instability can lead to significant vibrations and potential structural damage, the predictable aspect of galloping motions presents an opportunity for energy harvesting, especially in applications involving flexible, elongated structures [21].

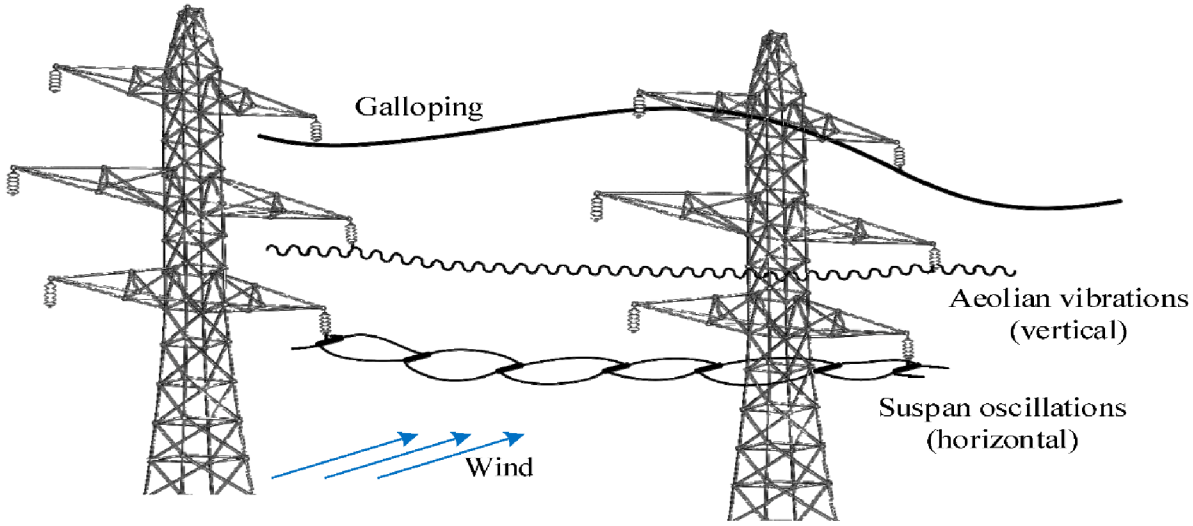

Figure 3 Galloping [23]

Flutter

Aeroelastic flutter describes self-induced oscillations resulting from the interaction between aerodynamic forces and the elastic properties of a structure. It is commonly associated with aircraft wings and suspension bridges. Although flutter is generally undesirable in engineered structures due to its potential for catastrophic failure, the principles underlying flutter can inform the design of energy harvesting systems that utilise piezoelectric materials to convert mechanical vibrations into electrical energy [21].

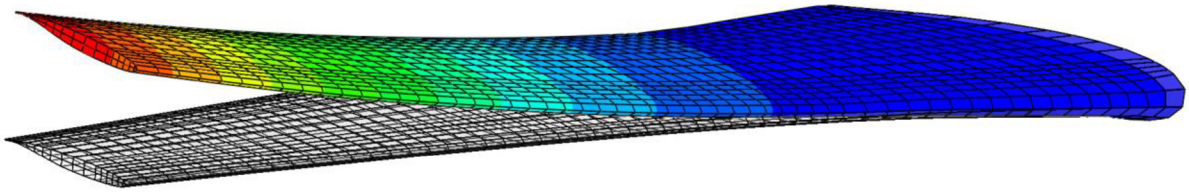

Figure 4 Flutter [24]

Turbulence-Induced Vibration

Turbulence-induced vibrations are caused by the interaction of structures with turbulent fluid flows. The random fluctuations in fluid velocity and pressure associated with turbulence can induce vibrations in structures. While this category of FIV presents challenges for energy harvesting due to the random nature of the vibrations, it also offers a broad spectrum of

opportunities for capturing energy from environmental flows, such as in riverine or oceanic contexts [21].

1.3.2. Factors Affecting Flow-Induced Vibrations

Several factors play a critical role in determining the nature and extent of vibrations induced by fluid flow. These factors include flow characteristics, fluid properties, object geometry and properties, fluid-structure interaction dynamics, surface conditions, and operational conditions [20]. A comprehensive understanding of these factors is essential for optimising the design of structures for both vibration mitigation and energy harvesting applications [21].

1.3.3. Energy Harvesting Innovations

While safety remains paramount, exploring energy harvesting opportunities within energy facilities is essential. The use of piezoelectric elements allows us to convert mechanical vibrations resulting from FIV into electrical energy [25]. These elements can be strategically integrated into structures, capturing energy from flow-induced motions.

By integrating these applications, we strike a balance between safety, efficiency, and sustainability in the dynamic landscape of energy production and distribution.

Flow-induced vibrations (FIV) encompass a diverse range of phenomena that have substantial implications for both structural integrity and the innovative harvesting of renewable energy. Examining FIV from the perspective of energy harvesting, especially utilisation of piezoelectric elements, reveals an exciting intersection between fluid dynamics and renewable energy technology. As the world increasingly seeks sustainable energy solutions, understanding and applying flow-induced vibrations will undoubtedly play a pivotal role in harnessing the power of natural fluid flows.

1.4. Literature Review about Harvesting of Flow-Induced Vibrations using Piezoelectric Materials

Wake-Induced Vibrations in Circulating Water Channel

Sustainability underscores the necessity for innovative approaches to ocean exploration. Autonomous underwater vehicles (AUVs) are pivotal in this endeavour, but their effectiveness is hindered by limited cruising ranges due to factors such as water resistance and battery capacity. Addressing this challenge, Nishi et al. proposed an energy harvesting system capable of powering AUVs underwater. This system harnesses energy from seawater currents, enabling AUVs to charge their batteries in situ without the need to resurface. To validate their concept, they constructed an experimental setup comprising a submerged cylinder stimulated by vortex-induced forces (wake-induced vibration) and a generator driven by the cylinder's motion. Optimising the cylinder's diameter to maximise lift force, they also positioned a fixed cylinder adjacent to the moving one to enhance synchronisation range and amplitude. Results demonstrate that these design features significantly enhance energy conversion efficiency, offering promising advancements in utilising wake-induced vibration for sustainable underwater energy harvesting [26].

Piezoelectric Energy Harvesting from Flow Induced Vibrations

Wang, D.-A., and Ko, H.-H. developed a piezoelectric energy harvester that utilizes the oscillation of a piezoelectric film to convert flow energy into electrical energy. They crafted a finite element model to predict the voltage generated by the piezoelectric laminate under a distributed load, enabling the analysis of variables such as piezoelectric film dimensions and fluid pressure. Experimental testing of prototypes yielded an open-circuit output voltage of 2.2 V peak-to-peak and an instantaneous output power of 0.2 μW under specific excitation pressure oscillations. The consistency between the experimental results and the model predictions confirms the accuracy of the finite element model. These energy harvesters show potential for autonomously powering miniature devices in challenging environments, thereby decreasing dependence on finite power sources and reducing maintenance needs. The research provides valuable insights into the optimisation of piezoelectric energy harvesters for capturing energy from flow-induced vibrations [27].

Piezoelectric Vortex Induced Vibration Energy Harvesting in a Random Flow Field

This study by Adhikari et al. develops and analyses a mathematical model for a piezoelectric cantilever beam with an end mass designed to harvest energy from vortex shedding-induced vibrations at its free end. It explores both deterministic and stochastic excitation scenarios, integrating mechanical and electrical models to evaluate energy output. Under deterministic conditions, the research examines performance without randomness, while a random process model considers uncertainty and weakly stationary conditions. Results highlight optimal configurations, particularly the use of an inductor for maximising power output under random excitations. The findings are significant for designing VIV-based piezoelectric energy harvesters suitable for micro-scale devices, wireless sensor networks, and low-power electronics, enhancing understanding of system optimisation under varying flow conditions [28].

Exploring the Efficiency of Piezoelectric Actuators in Energy Harvesting from Internal Flows: A Numerical Approach by Sarviha et al.

In this study, Sarviha et al. investigate the potential of piezoelectric (PZT) actuators for energy harvesting from steady internal flows, focusing on wake-induced vibration (WIV). Conducting simulations at a Reynolds number of 200, the researchers examine the effects of various blockage ratios ranging from 0.08 to 0.5. This research identifies the optimal placement of the PZT actuator, aiming to maximise the energy harvested by exploiting the lift force variations caused by different confinement levels. The PZT and the diaphragm hosting it are respectively modelled as cantilever and fixed-fixed structures to realistically simulate their interaction with the fluid flow. The study determines key spacing ratios that are crucial for optimising the harvester's performance. The results provide significant insights into the fluid-structural interactions within these systems, offering valuable, practical design guidelines for developing efficient energy harvesting systems. These findings are especially relevant for the design of self-sufficient energy solutions in remote sensing applications, proposing a sustainable approach to powering devices in locations where traditional energy sources are unfeasible [6].

1.5. The goal of this work

The primary objective of this work is to investigate the potential of harvesting energy from flow-induced vibrations using a piezoelectric cylinder subjected to airflow. This involves a detailed experimental setup including a piezoelectric element, support structures, an airflow source, and a PXI data acquisition system. The setup is designed to optimise the exposure of the piezoelectric cylinder to airflow and maximise energy capture. Measurements focus on airflow characteristics, optimal positioning, valve settings, and the relationship between airflow speed and generated voltage. The results aim to provide insights into this setup, practical applications, and future enhancements in piezoelectric energy harvesting systems.

2. Experimental Setup

The experimental setup described herein is designed to investigate the potential of harvesting energy from flow-induced vibrations using a piezoelectric cylinder subjected to airflow. This chapter details the components and arrangement of the setup, which includes a piezoelectric element, support structures, an airflow source, and instrumentation for data acquisition. Figure 5 shows the setup of the experiment.

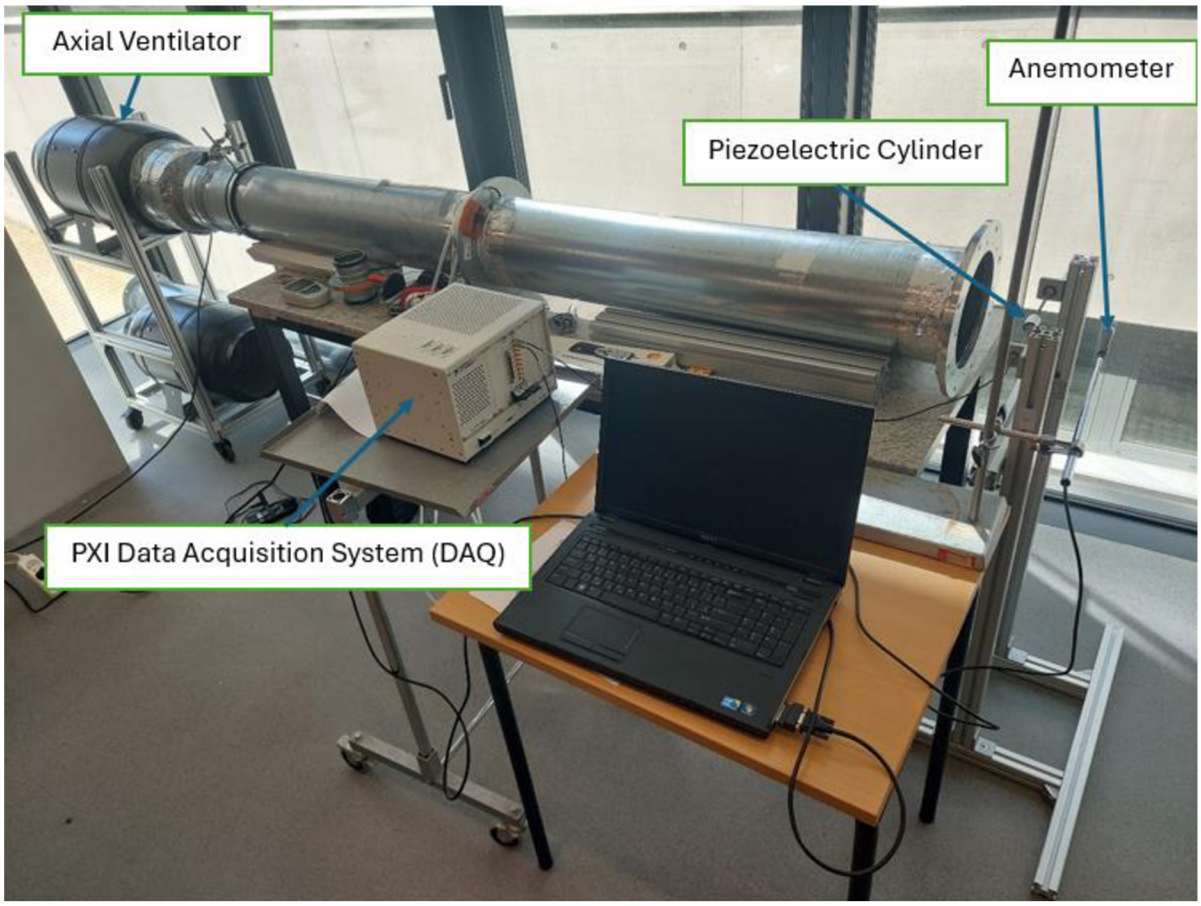

Figure 5 Experimental Setup

Components

Piezoelectric Cylinder

The core component of the experiment, the piezoelectric cylinder, is fabricated from PZT-5A, a material known for its high piezoelectric sensitivity and response to mechanical stress. The dimensions and properties of the PZT-5A piezoelectric cylinder are summarized in Table 1.

Table 1 Dimensions and Properties of PZT-5A Piezoelectric Cylinder [29]

Dimensions

Length	30 mm
External Diameter	20 mm
Thickness	1 mm
Properties	
Dielectric Constant (1kHz)	~1800
Dielectric Loss Factor (1kHz) (Tanδe)	~0.02%
Clamped Dielectric Constant Density	~900 g/cm³
Curie Point (Tc)	350°C
Mechanical Quality Factor (Qm)	~80
Coercive Field (Measured < 1Hz)	12.0 kV/cm
Remanent Polarization (Pr)	39.0 μCoul/cm²
Coupling Coefficients	k31: 0.35, kt: 0.49, k15: 0.61
Piezoelectric Charge Coefficient (d31)	-190 Coul/N x 10^{-12}
Piezoelectric Charge Coefficient (d33)	390 Coul/N x 10^{-12}
Piezoelectric Charge Coefficient (d15)	460 Coul/N x 10^{-12}

Threaded Cylindrical Rod

Supporting the piezoelectric cylinder is a threaded cylindrical rod, which acts both as a structural backbone and a medium for assembly. The rod is an M5 thread, facilitating fastening of the PZT-5A cylinder with nuts and washers. This rod is designed to pass directly through the piezoelectric cylinder, facilitating a secure and centralized mounting, crucial for uniform vibration transmission. Table 2 summarizes the dimensions of the rod.

Table 2 Dimensions of the Threaded Cylindrical Rod

Component	Length (mm)	Diameter (mm)	Additional Specification
Threaded Cylindrical Rod	150	5	M5 thread

PXI Data Acquisition System (DAQ)

The data acquisition for this experiment is managed using a PXI-1033 DAQ system by National Instruments. The PXI-1033 is chosen for its high-speed and high-resolution capabilities, which are essential for detecting and recording the subtle fluctuations in electrical output generated by the piezoelectric cylinder. The system is interfaced with a laptop, enabling real-time monitoring and dynamic adjustment of experimental parameters, thus facilitating precise data recording and further analysis.

Mounting and Assembly

Assembly Arrangement

Figure 6 shows the positioning of the piezoelectric cylinder in the experimental setup.

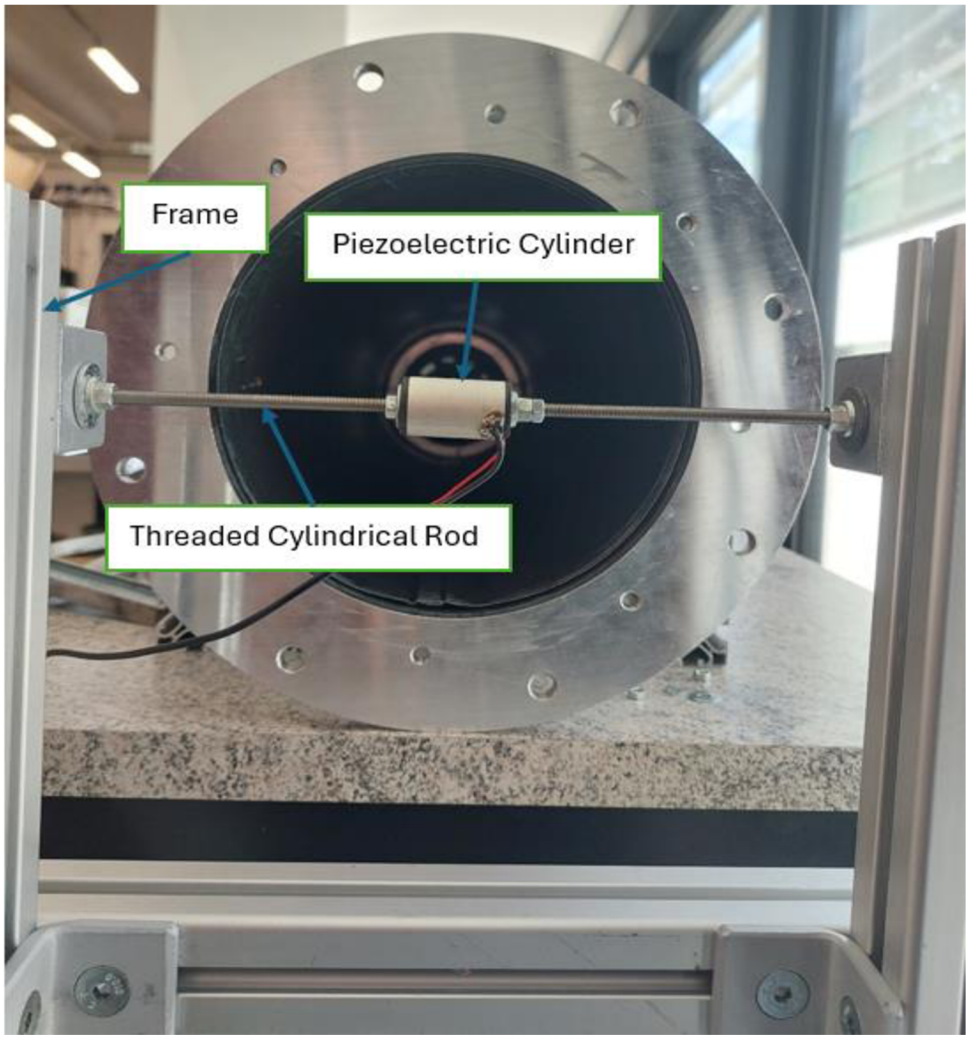

Figure 6 Cylinder Configuration

The experimental assembly is methodically arranged to optimise the exposure of the piezoelectric cylinder to airflow-induced vibrations. The setup involves the following configuration:

- The piezoelectric cylinder is centrally mounted on the threaded cylindrical rod.
- Plastic side walls are utilized to hold the piezoelectric cylinder in place, secured tightly with nuts to eliminate any lateral movements.
- The cylindrical rod is supported at both ends by a robust frame, ensuring the assembly's stability during the experiment.
- Rubber was used under the frame for damping vibrations.

Positioning Relative to Airflow

The entire assembly is positioned horizontally and laterally in front of an axial ventilator's outlet, where a pipe of 20cm internal diameter directs the airflow. This orientation ensures that the piezoelectric cylinder is subjected to a consistent and direct flow, inducing optimal vibrational response for energy harvesting.

Blockage Ratio

The blockage ratio is calculated as the ratio of the cross-sectional area of the piezoelectric cylinder to the cross-sectional area of the pipe outlet. For the piezoelectric cylinder used in this experiment, with a diameter of 20 mm and pipe diameter of 20 cm, the blockage ratio is 0.019 or 1.9%. This indicates minimal obstruction to the airflow, ensuring effective experimentation with negligible disruption [30].

This described experimental setup is used to explore the energy harvesting capabilities of a piezoelectric cylinder exposed to flow-induced vibrations. The choice of materials, component dimensions, and assembly arrangement are all tailored to maximise the vibrational response and subsequent energy generation. The setup's effectiveness and the accuracy of data collected are ensured by sophisticated instrumentation and a well-thought-out configuration, setting the stage for rigorous experimentation.

3. Air Speed Measurement

The experimental process began with the determination of the necessary sampling time, where appropriate time intervals were established to ensure accurate and reliable data collection. Following this, the determination of the speed profile at various locations was conducted to map the airflow characteristics and identify optimal positions for placing the piezoelectric cylinder. Once the speed profile was established, the next step involved the measurement of air speed at various k values. Here, air speed was measured at different valve settings (k values) to understand how airflow varied with valve adjustments.

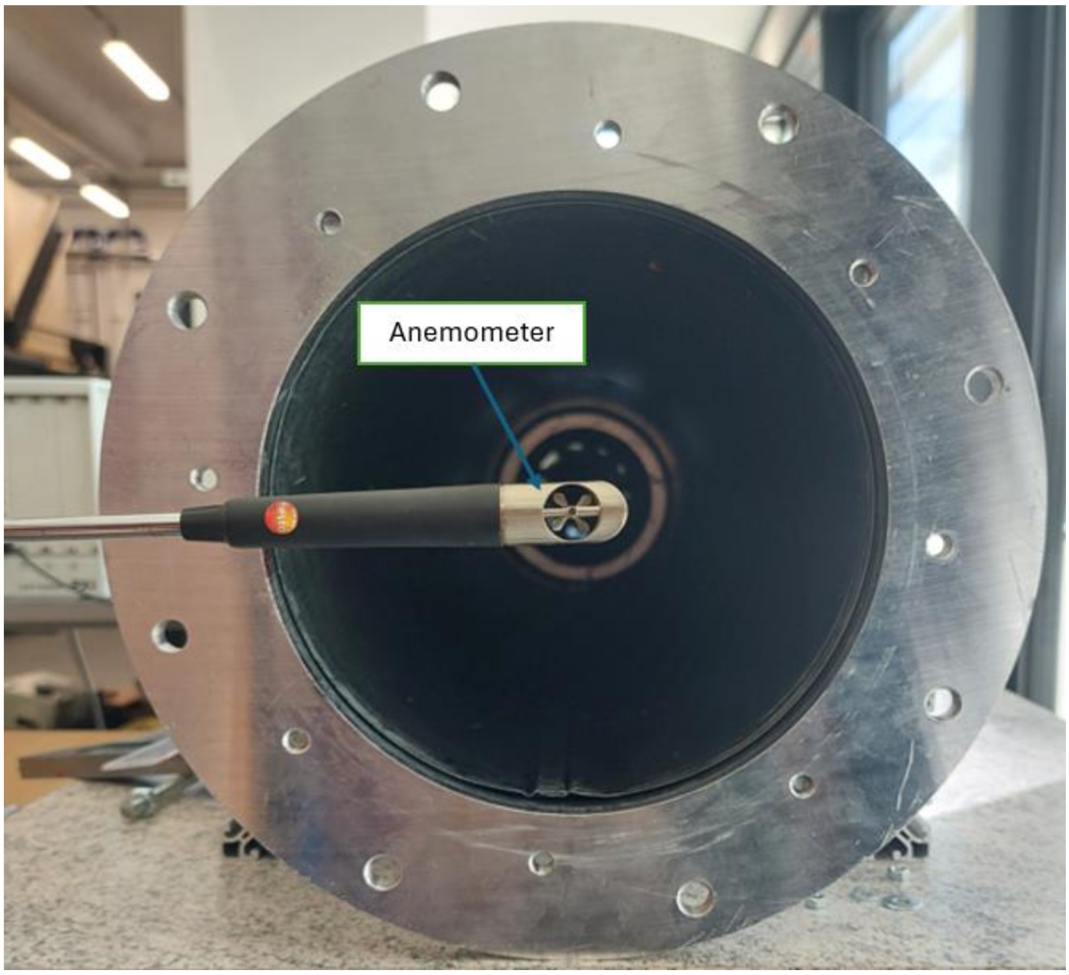

Figure 7 Anemometer Positioning

3.1. Determination of the Necessary Sampling Time

The Measurement Stability Test was conducted to ensure the accuracy and reliability of flow velocity measurements obtained via an anemometer in the experimental setup. Given the critical role of airflow velocity in the study of energy harvesting from flow-induced vibrations,

the precision of flow measurements cannot be overstated. The anemometer exhibited fluctuating readings, necessitating a methodology to determine the optimal time duration over which to average these readings to achieve a stable and reliable mean value.

To determine the most suitable averaging period for the anemometer readings, a stability test was conducted. The anemometer's probe was positioned 4 cm downstream of the pipe's outlet and 8 cm laterally from the centre of the airstream.

The test involved recording the air speed at several time intervals, progressively increasing the duration over which the readings were averaged. At each duration, the measurement was repeated five times for repeatability. The primary variables recorded in each test iteration were the individual air speed measurements, the calculated average air speed, the total duration of the measurement period, and the standard deviations.

Table 3 summarises the results obtained during the stability test. All measurements of speed and time on this table are in metres and seconds, respectively.

Table 3 Speed Measurement Stability Test

Air Speed 1	Air Speed 2	Air Speed 3	Air Speed 4	Air Speed 5	Average Air Speed	Time	Standard Deviation of Air Speed	Time Duration	Avg Air Speed
4.9	5	5.4	5.5	5.3	5.22	1	0.23152	1	5.22
5.3	5.3	5.4	5	4.8	5.16	2	0.2245	2	5.16
5.1	5	5.1	5.2	5.4	5.16	5	0.13565	5	5.16
5	5.2	5.2	5.2	5.1	5.14	10	0.08	10	5.14
5	5.2	5.1	5	5.2	5.1	20	0.08944	20	5.1
5.2	5.1	5.1	5.2	5.2	5.16	30	0.04899	30	5.16
5.1	5.1	5.1	5.1	5.1	5.1	40	0	40	5.1
5.1	5.1	5.1	5.1	5.1	5.1	50	0	50	5.1
5.1	5.1	5.1	5.1	5.1	5.1	60	0	60	5.1
5.1	5.1	5.1	5.1	5.1	5.1	70	0	70	5.1
5.1	5.1	5.1	5.1	5.1	5.1	80	0	80	5.1
5.1	5.1	5.1	5.1	5.1	5.1	90	0	90	5.1
5.1	5.1	5.1	5.1	5.1	5.1	100	0	100	5.1
5.1	5.1	5.1	5.1	5.1	5.1	110	0	110	5.1
5.1	5.1	5.1	5.1	5.1	5.1	120	0	120	5.1

Figure 8 presents the results of the stability test to determine the optimal sampling time for average air speeds. The results indicate that while shorter measurement durations (less than 10 seconds) yield higher standard deviations, indicating significant fluctuation in readings, the standard deviation decreases markedly as the averaging period increases. Notably, the standard deviation reaches zero at 40 seconds, with subsequent longer durations maintaining this stability.

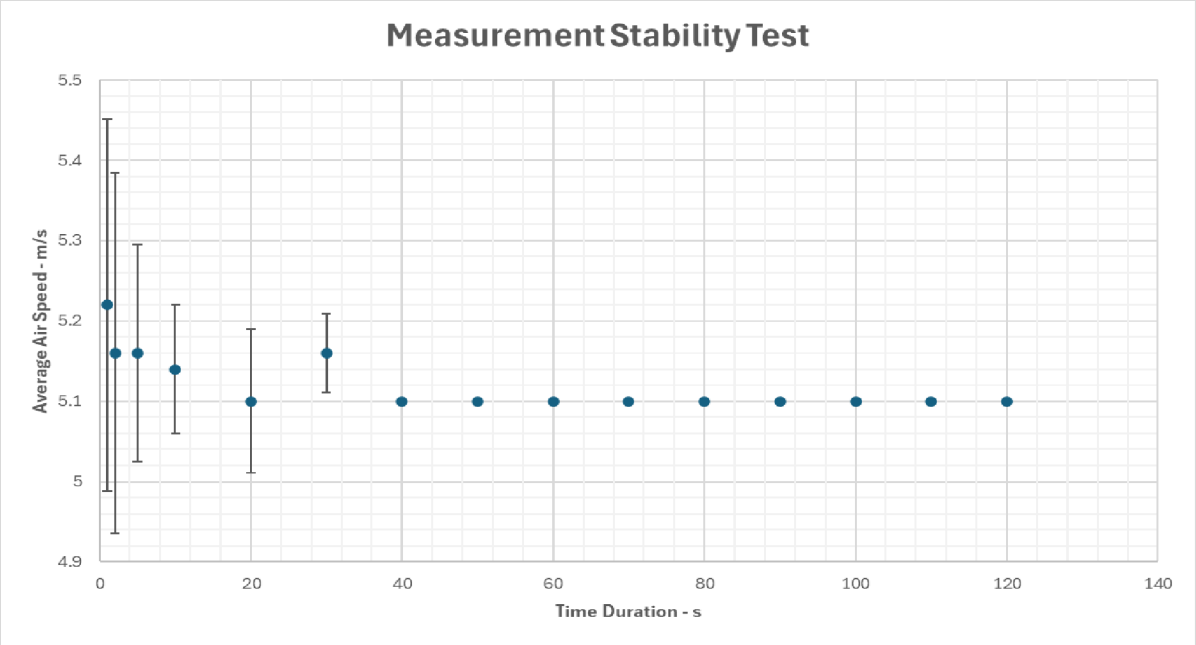

Figure 8 Speed Measurement Stability Test

Based on the conducted tests, it is evident that mean values of airflow speed become stable and reliable when averaged over a duration of 50 seconds. This duration provides a consistent average air speed measurement with minimal variability, suitable for the experimental objectives laid out in this study. Hence, subsequent airflow velocity measurements for energy harvesting experiments will employ this 50-second averaging period to ensure accuracy and reproducibility in data acquisition.

These findings are vital for ensuring that the data collected in further experiments is robust, providing a solid basis for analysing the effects of airflow-induced vibrations on the energy harvesting capabilities of piezoelectric materials.

3.2. Determination of the Speed Profile at Various Locations

Speed measurements were conducted at different distances from the outlet of the axial ventilator, and at various radii across the output pipe, to map the flow characteristics and identify the most uniform flow region.

The primary goal of this experiment was to determine the best location to position the piezoelectric cylinder by analysing the airflow speed profile at different points. This involved:

- Measuring air speeds at various lateral positions across a 10 cm radius of the output pipe.
- Assessing the flow uniformity at different axial distances (2 cm, 4 cm, 6 cm, and 8 cm) from the outlet of the axial ventilator.
- Identifying the point where the airflow is most uniform, which is critical for maximising the efficiency of the piezoelectric energy harvesting.

Procedure

The experimental setup involved the following steps:

Equipment Setup: The axial ventilator was set to low-speed mode to ensure consistent airflow.

Measurement Points: Air speed measurements were taken at lateral intervals of 1 cm across the radius of the output pipe (0 to 10 cm), and at axial distances of 2 cm, 4 cm, 6 cm, and 8 cm from the outlet.

Data Collection: At each measurement point, air speed was recorded five times to ensure accuracy and to calculate average speeds and standard deviations.

The specific steps for each axial distance were as follows:

The anemometer was positioned at the specified axial distance (2 cm, 4 cm, 6 cm, or 8 cm) from the outlet. The air speed was measured at lateral positions from 0 cm to 10 cm at 1 cm intervals (also expressed as r/R, where r is distance from the centre of the air stream and R is the radius of the outlet pipe from the axial ventilator, both in cm).

Five air speed readings were taken at each position.

Results

Figure 9 shows the variation of speed vs position from the centre of the air stream. For each axial distance from the outlet, the results were recorded and presented on a graph, with radius r/R (distance from the centre in cm divided by the 10 cm radius of the outlet pipe) plotted against the average air speed in m/s.

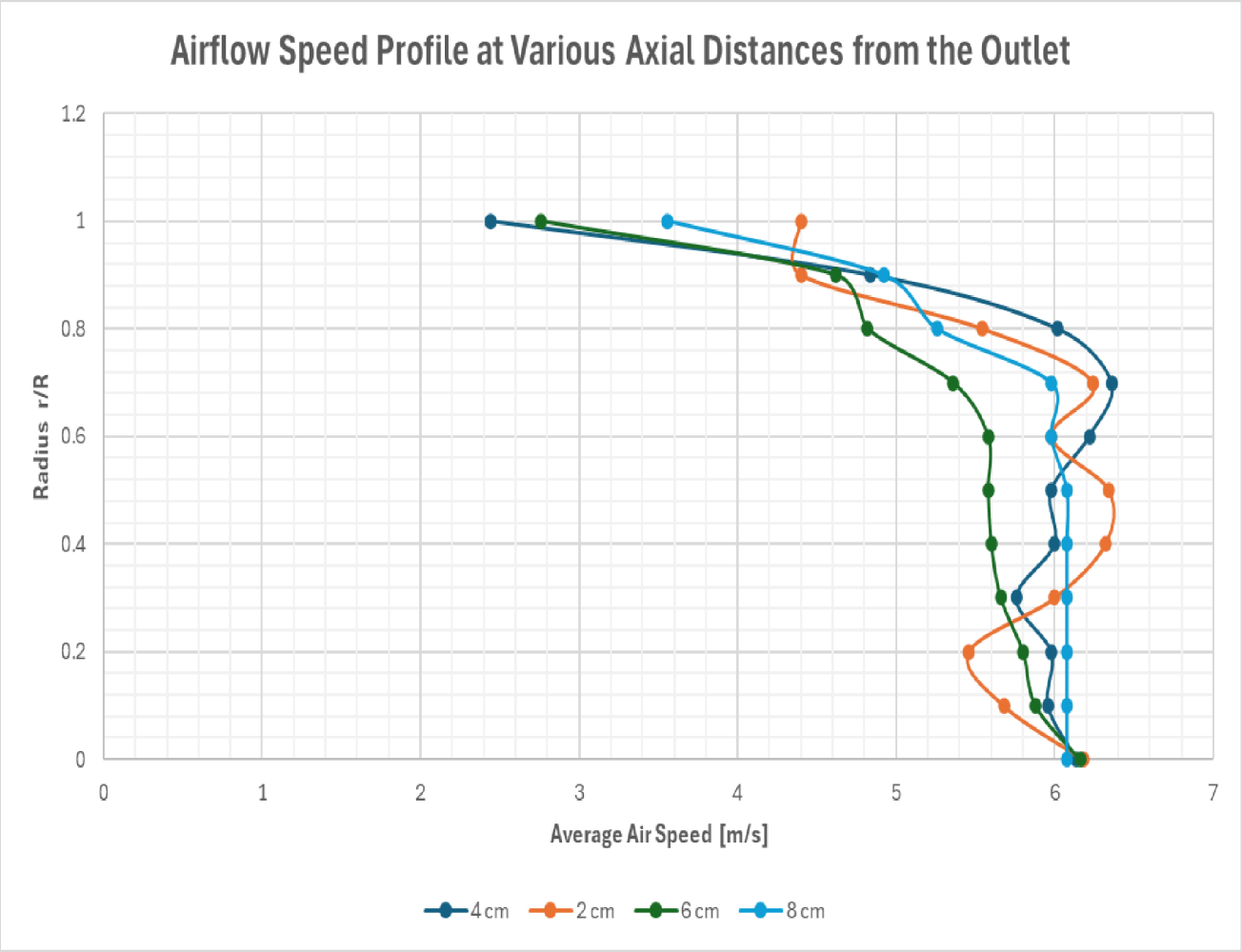

Figure 9 Airflow Speed Profile at Various Axial Distances from the Outlet

Discussion

The speed profiles at different axial distances highlight the variation in airflow uniformity.

2 cm from the outlet: The flow shows significant variation, particularly at the outer radii (for r/R 0.9 to 1), indicating a less uniform flow.

4 cm from the outlet: The flow becomes slightly more uniform, but there is still noticeable variation, especially at larger radii.

6 cm from the outlet: The airflow continues to show improved uniformity, though there are still fluctuations.

8 cm from the outlet: This distance demonstrates the most uniform flow profile, with consistent speeds across the majority of the radius and lower standard deviation of the air speed.

Based on the experimental data, it is evident that the most uniform airflow occurs at 8 cm from the outlet of the axial ventilator. This location minimises flow disturbances and provides a stable environment for the piezoelectric cylinder, enhancing the efficiency of energy harvesting from flow-induced vibrations. Thus, for practical applications, the piezoelectric cylinder should be positioned at this distance for stable measurements.

3.3. Measurement of Air Speed at Various k Values

The goal of this experiment was to assess air speed at different valve settings (referred to as k values) for both high and low-speed modes of the axial ventilator. Understanding how air speed changes with varying valve positions is essential for optimising the placement and effectiveness of piezoelectric elements used to harvest energy from flow-induced vibrations.

Procedure:

Variables

- **Independent Variable**: Valve setting (k), ranging from 0 to 8.
- **Dependent Variable**: Measured air speed at the centre of the air stream, 8 cm in front of the outlet pipe from the axial ventilator.
- **Controlled Variables**:
    - Distance from the outlet pipe (8 cm)
    - Position in the air stream (centre)
    - Ventilator speed mode (high and low)

1. **Setup of the Measurement Apparatus**:

   The air speed measurement device (anemometer) 8 cm was positioned in front of the outlet pipe from the axial ventilator, ensuring it was in the centre of the air stream.

2. **Measurement at Low-Speed Mode**:

   The ventilator was set to low-speed mode.

   The air speed was recorded at different valve settings (k values 0, 1, 1.5, 2, 2.5, ..., 8). 5 measurements were taken at each setting to calculate the average and standard deviation.

3. **Measurement at High-Speed Mode**:

   The procedure described above was repeated, but with the ventilator set to high-speed mode. The air speed for each k value was recorded and the corresponding standard deviation was calculated.

4. **Data Recording and Analysis**:

   The collected data was organised into tables for both low and high-speed modes.

   A scatter graph was plotted to visualise the relationship between valve settings (k values) and measured air speed.

Results

Figure 10 shows the variations of air speed at different valve settings (referred to as k values) for low and high-speed modes. It can be noticed that from k values 8 to 4, the air speed increases linearly then drops. It was expected that from k values 8 to 0, the speed would continue to increase linearly, but instead, it dropped.

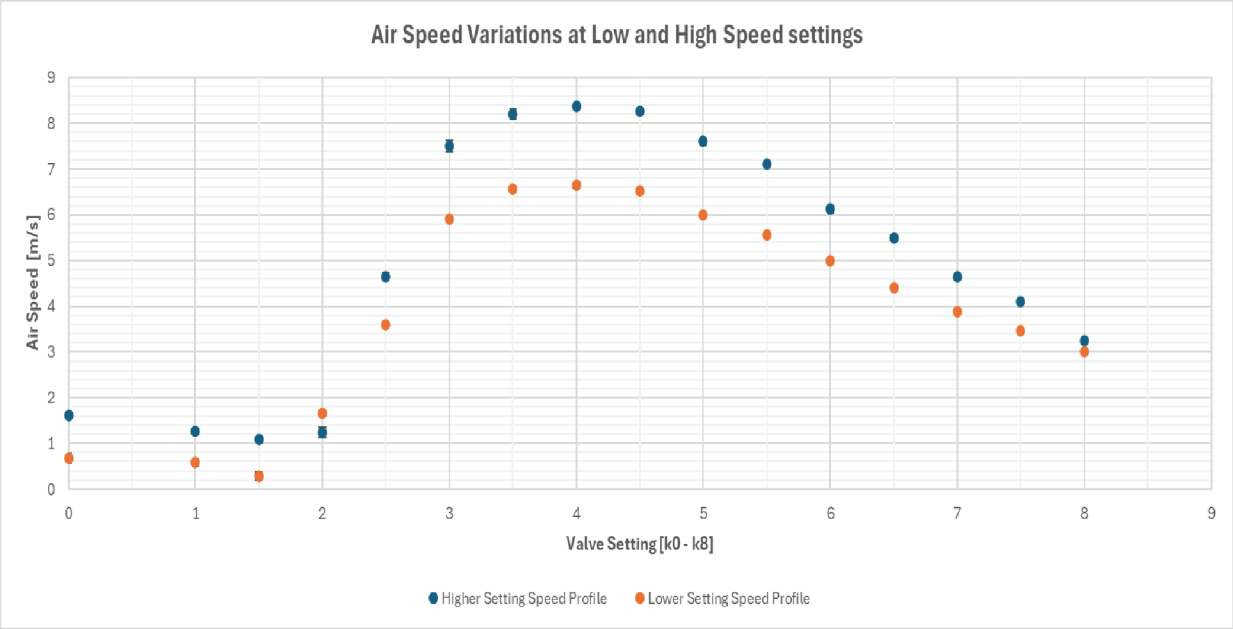

Figure 10 Air Speed Variations at Low and High-Speed Settings

Analysis of Results

Low-Speed Mode: Focusing on the linear region, Figure 11 shows the relationship between air speed and valve settings.

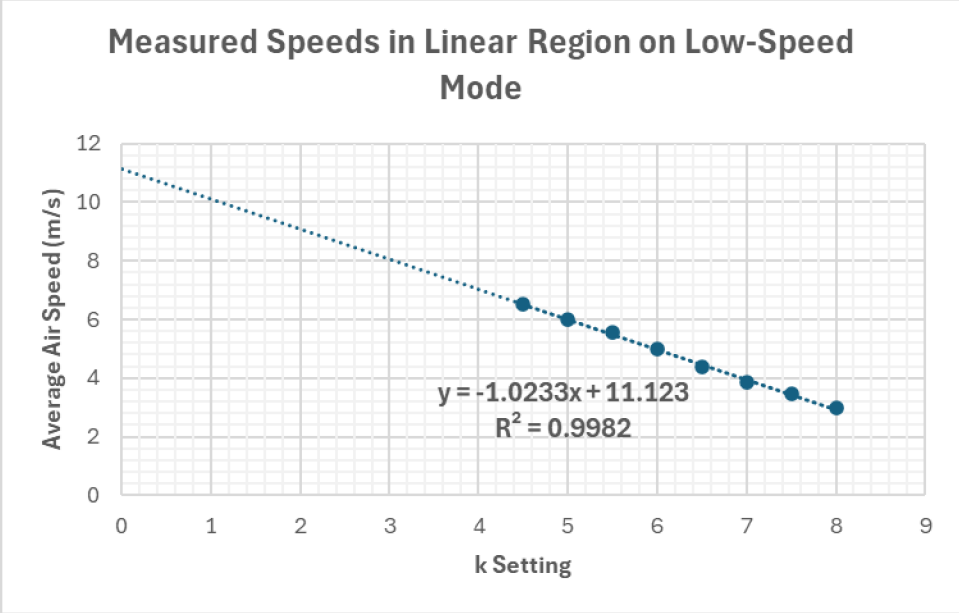

Figure 11 Average Speeds in Linear Region on Low-Speed Mode

- From k = 8 to k =4, measured air speed increased almost linearly with decreasing k values, reaching its maximum at k = 4 with a speed of 6.64 m/s.
- Below k = 4, the air speed begun to decrease, and the flow characteristics changed
- The standard deviation was generally low, indicating consistent measurements, except for k = 0 and k = 1.5, where slight variations occurred.

High-Speed Mode: Focusing on the linear region, Figure 12 shows the relationship between air speed and valve settings.

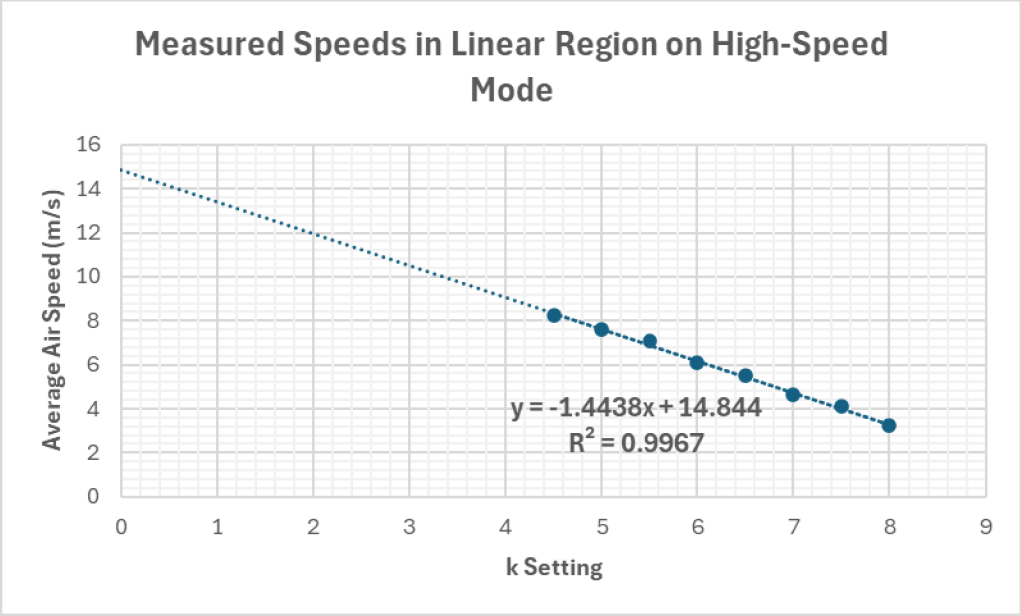

Figure 12 Average Speeds in Linear Region on High-Speed Mode

- From k = 8 to k =4, the measured air speed increased more rapidly with decreasing valve setting K compared to low-speed mode, reaching its maximum at k = 4 with a speed of 8.38 m/s.
- Similar to the low-speed mode, the air speed decreased below k = 4
- was higher at certain k values (e.g., k = 2, k = 3), indicating more variability in measurements at higher speeds.

Both speed modes show a maximum air speed around k = 4. The variations in air speed and standard deviation across different k values provide insights into the flow characteristics of the

air supplied, crucial for designing efficient energy harvesting systems. This experiment demonstrates the relationship between valve settings and air speed from the axial ventilator.

4.Piezoelectric Voltage Measurement

The goal of this experiment was to detail the measurement of voltage generated by the piezoelectric cylinder when exposed to airflow at different speeds and valve settings (k values). The analysis focuses on understanding the relationship between airflow-induced vibrations and the resultant voltage, particularly the root mean square (RMS) voltage, which is critical for assessing the efficiency of energy harvesting.

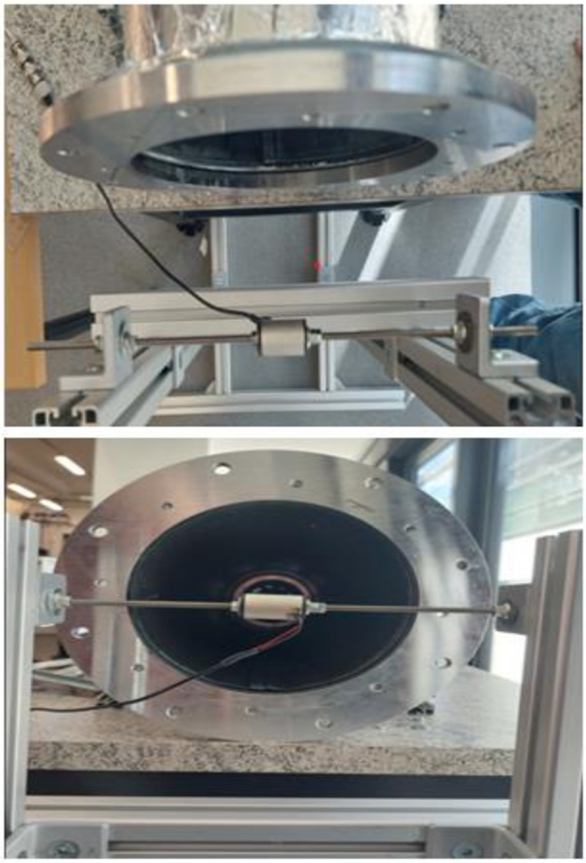

Figure 13 Piezoelectric Cylinder Setup

Procedure

The experimental setup was maintained as described in the previous chapters, with the piezoelectric cylinder positioned at the optimal location determined earlier (8 cm from the outlet of the axial ventilator). Measurements were conducted in both low-speed and high-speed modes of the ventilator, and the resulting data was exported to Excel for analysis.

Variables:

- **Independent Variable**: Valve setting (k values ranging from 0 to 8)
- **Dependent Variables**: Measured air speed, average voltage, RMS voltage, standard deviation of voltage, average noise, noise RMS, and noise standard deviation
- **Controlled Variables**: Distance from the outlet pipe (8 cm), position in the air stream (centre), and ventilator speed mode (high and low)

Steps:

1. **Measurement of Noise**: Noise refers to any unwanted electrical signals or disturbances that can interfere with the measurement of the actual signal of interest. In this context, noise could be caused by various factors such as electrical interference from surrounding equipment, vibrations from the environment, or inherent electrical noise within the measurement system itself. Ambient noise was measured by measuring voltages without air flow. Measuring ambient noise is essential to ensure that subsequent measurements accurately reflect the piezoelectric cylinder's response to airflow, rather than being influenced by these extraneous signals.
2. **Positioning**: The piezoelectric cylinder was positioned 8 cm in front of the outlet pipe, ensuring it was centred in the airstream.
3. **Data Collection**: Voltage measurements were taken at various valve settings in both low and high-speed modes:
    - **Low-Speed Mode**: Air speed and voltage were recorded for k values 0, 1, 1.5, 2, 2.5, ..., 8.
    - **High-Speed Mode**: The procedure was repeated for high-speed mode.
4. **Measurement Repetition**: Three measurements were taken at each setting to calculate average values and standard deviations.
5. **Data Recording**: The collected data was organized into tables for both speed modes. Scatter graphs were plotted versus k, air speed, and Reynolds number to visualize the relationships between the variables.

Results

Low-Speed Mode:

Table 4 presents the measured air speed, average voltage, RMS voltage, standard deviation of voltage, average noise, noise RMS, and noise standard deviation for each valve setting (k value) on low-speed mode. Additionally, it includes the calculated Reynolds number and RMS standard deviation. The values of the coefficient of dynamic viscosity and density of air used in the calculations of are 1.825×10^{-5} Pascal-seconds (Pa·s) and 1.204 kg/m^3, respectively.

Table 4 Low Speed Piezoelectric Voltage Measurements

Valve Setting (k)	Speed (m/s)	Avg Voltage (mV)	RMS Voltage (mV)	STD Voltage (mV)	Avg Noise (mV)	Noise RMS (mV)	Noise STD (mV)	Reynolds No.	RMS STD (mV)
8	3	-1.6163	5.8402	5.6104	-2.2231	5.9965	5.5673	3958.36	6.28E-05
7.5	3.46	-1.6184	5.8251	5.5957	-2.2231	5.9965	5.5673	4565.3	1.27E-05
7	3.88	-1.9973	5.9418	5.5952	-2.2231	5.9965	5.5673	5119.47	3.13E-05
6.5	4.4	-1.4833	5.8107	5.617	-2.2231	5.9965	5.5673	5805.59	4.68E-05
6	5	-2.2071	5.9959	5.5743	-2.2231	5.9965	5.5673	6597.26	3.16E-05
5.5	5.56	-2.5242	6.1315	5.5865	-2.2231	5.9965	5.5673	7336.15	6.69E-05
5	6	-2.3553	6.0543	5.5728	-2.2231	5.9965	5.5673	7916.71	5.46E-05
4.5	6.52	-1.9667	5.9176	5.5753	-2.2231	5.9965	5.5673	8602.83	0.00013
4	6.64	-1.9316	5.9198	5.5956	-2.2231	5.9965	5.5673	8761.16	8.53E-05
3.5	6.56	-2.0868	5.9729	5.5956	-2.2231	5.9965	5.5673	8655.61	4.04E-05
3	5.9	-2.0874	5.957	5.579	-2.2231	5.9965	5.5673	7784.77	0.00013
2.5	3.6	-1.8524	5.8937	5.5862	-2.2231	5.9965	5.5673	4750.03	0.00012
2	1.66	-2.0338	5.9466	5.5858	-2.2231	5.9965	5.5673	2190.29	3.95E-05
1.5	0.28	-2.1004	5.9613	5.5788	-2.2231	5.9965	5.5673	369.447	1.47E-05
1	0.58	-2.323	6.0391	5.5723	-2.2231	5.9965	5.5673	765.282	7.92E-05
0	0.68	-1.5001	5.8075	5.6043	-2.2231	5.9965	5.5673	897.227	5.20E-05

1. RMS Voltage vs. Measured Air Speed and Valve Setting (k)

   Figure 14 shows the RMS voltage variation with changes in air speed and k values and highlights regions of linearity and randomness.

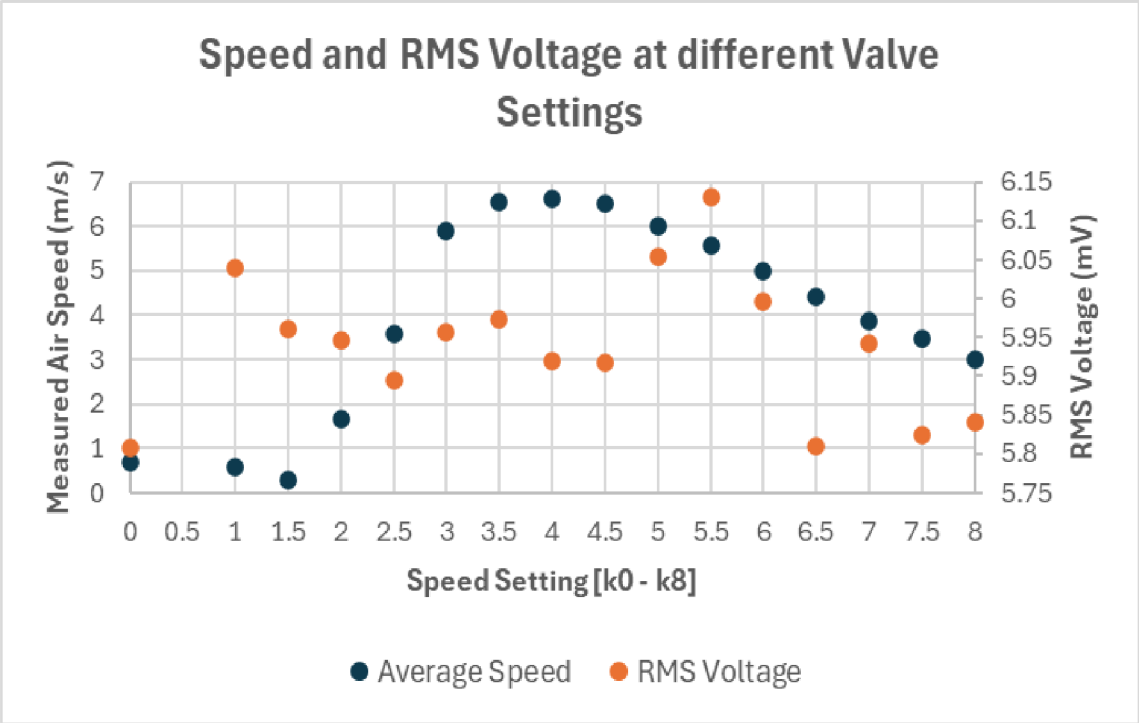

Figure 14 Variations of RMS Voltage and Measured Air Speed at different Valve Settings on Low-Speed Mode

2. RMS Voltage vs. Air speed in the Linear Region (k = 4 to 8)

   Figure 15 shows the variations of RMS voltage with air speed in the linear region.

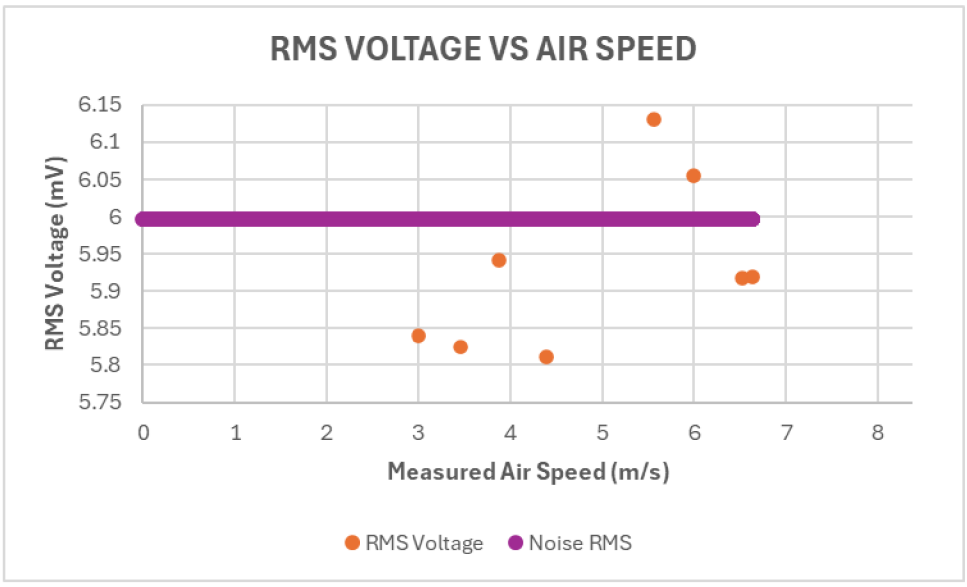

Figure 15 Variations of RMS Voltage with Measured Air Speed Low-Speed Mode

3. RMS Voltage vs. Reynolds Number in the Linear Region (k = 4 to 8)

   Figure 16 shows the variations of RMS voltage with the Reynolds number in the linear region.

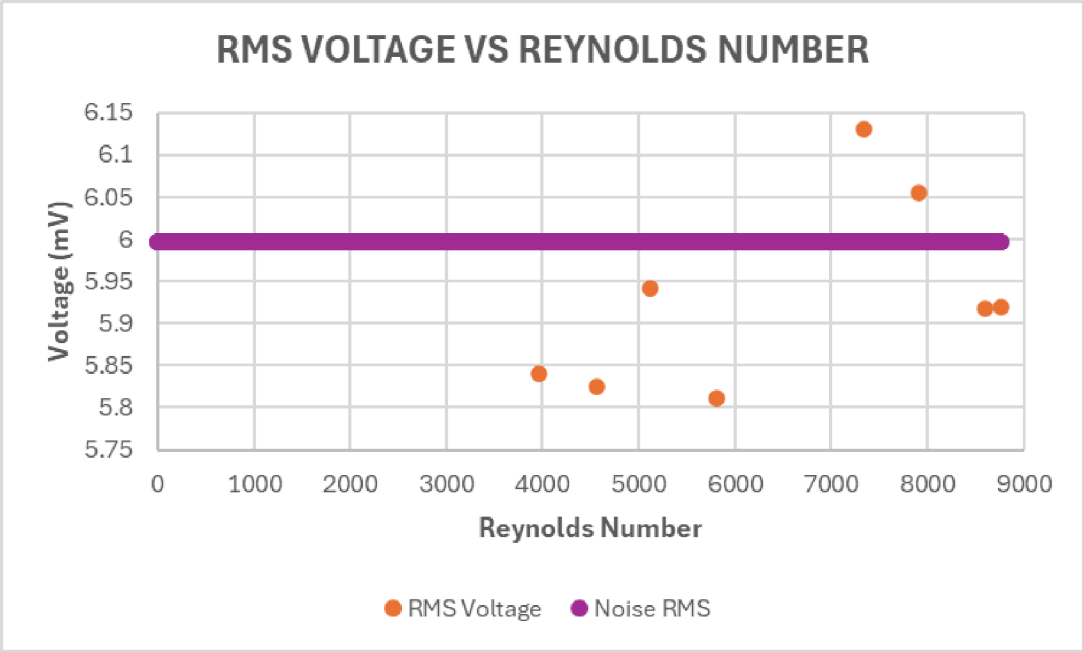

Figure 16 Variations of RMS Voltage with the Reynolds Number Low-Speed Mode

High-Speed Mode:

Table 5 presents the measured air speed, average voltage, RMS voltage, standard deviation of voltage, average noise, noise RMS, and noise standard deviation for each valve setting (k value) on high-speed mode. Additionally, it includes the calculated Reynolds number and RMS standard deviation. The values of the coefficient of dynamic viscosity and density of air used in the calculations of are 1.825×10^{-5} Pascal-seconds (Pa·s) and 1.204 kg/m^3, respectively.

Table 5 High Speed Piezoelectric Voltage Measurements

Valve Setting (k)	Speed (m/s)	Avg Voltage (mV)	RMS Voltage (mV)	STD Voltage (mV)	Avg Noise (mV)	Noise RMS (mV)	Noise STD (mV)	Reynolds No.	RMS STD (mV)
8	3.24	-1.6581	5.8298	5.5886	-2.9861	6.2977	5.5443	4275.02	6.28E-05
7.5	4.1	-2.1286	5.9837	5.5902	-2.9861	6.2977	5.5443	5409.75	1.27E-05
7	4.64	-1.7094	5.8722	5.617	-2.9861	6.2977	5.5443	6122.26	3.13E-05
6.5	5.5	-1.9854	5.9196	5.5756	-2.9861	6.2977	5.5443	7256.99	4.68E-05
6	6.12	-2.1804	6.0081	5.5942	-2.9861	6.2977	5.5443	8075.05	3.16E-05
5.5	7.1	-2.5522	6.1478	5.5929	-2.9861	6.2977	5.5443	9368.11	6.69E-05
5	7.6	-1.5763	5.8535	5.6293	-2.9861	6.2977	5.5443	10027.8	5.46E-05
4.5	8.26	-2.7834	6.2533	5.5963	-2.9861	6.2977	5.5443	10898.7	0.00013
4	8.38	-2.0095	5.9617	5.611	-2.9861	6.2977	5.5443	11057	8.53E-05
3.5	8.2	-3.2647	6.4756	5.5903	-2.9861	6.2977	5.5443	10819.5	4.04E-05
3	7.5	-2.7068	6.2295	5.6051	-2.9861	6.2977	5.5443	9895.89	0.00013
2.5	4.641	-3.0107	6.3545	5.5955	-2.9861	6.2977	5.5443	6123.58	0.00012
2	1.24	-2.5028	6.1458	5.6127	-2.9861	6.2977	5.5443	1636.12	3.95E-05
1.5	1.1	-3.193	6.4554	5.6094	-2.9861	6.2977	5.5443	1451.4	1.47E-05
1	1.26	-2.4017	6.1297	5.6381	-2.9861	6.2977	5.5443	1662.51	7.92E-05
0	1.62	-2.351	6.1242	5.6539	-2.9861	6.2977	5.5443	2137.51	5.20E-05

1. RMS Voltage vs. Measured Air speed and Valve Setting (k)

   Figure 17 shows the RMS voltage variation with changes in air speed and k values and highlights regions of linearity and randomness.

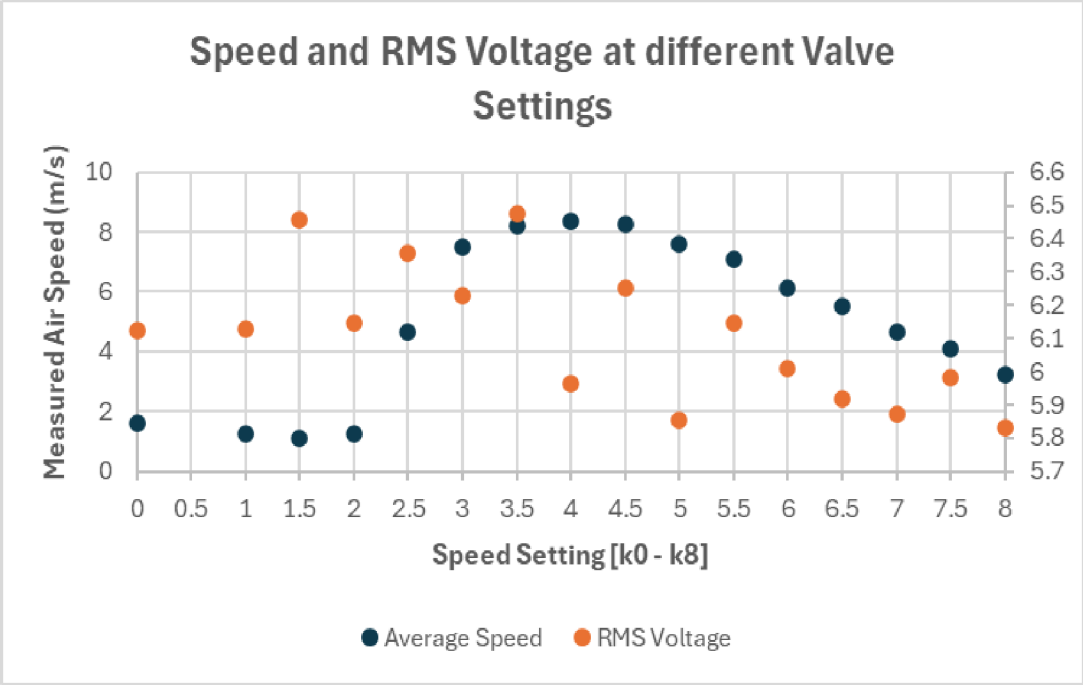

Figure 17 Variations of RMS Voltage and Measured Air Speed at different Valve Settings on High-Speed Mode

2. RMS Voltage vs. Air speed in the Linear Region (k = 4 to 8)

   Figure 18 shows the variations of RMS voltage with air speed in the linear region.

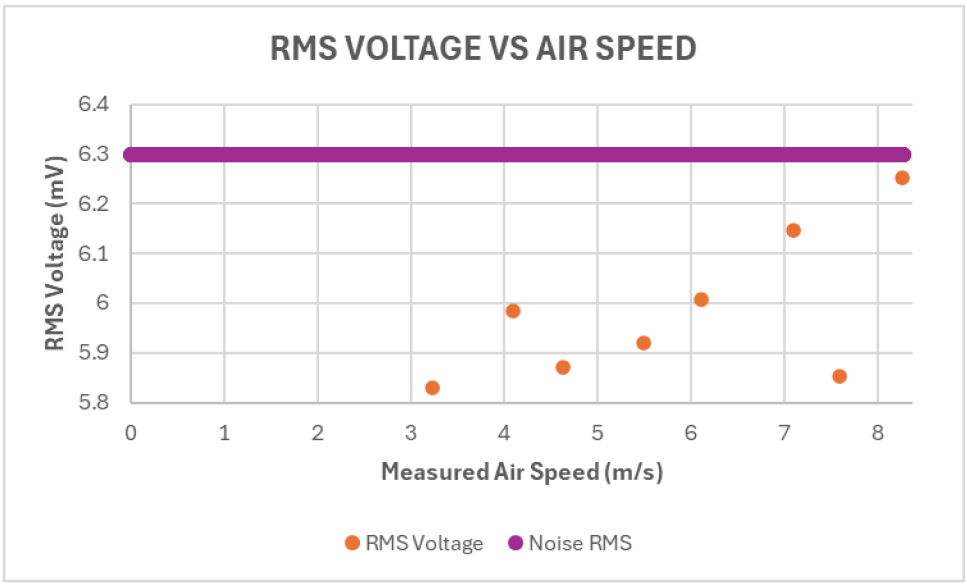

Figure 18 Variations of RMS Voltage with Measured Air Speed High-Speed Mode

3. RMS Voltage vs. Reynolds Number in the Linear Region (k = 4 to 8)

   Figure 19 shows the variations of RMS voltage with the Reynolds number in the linear region.

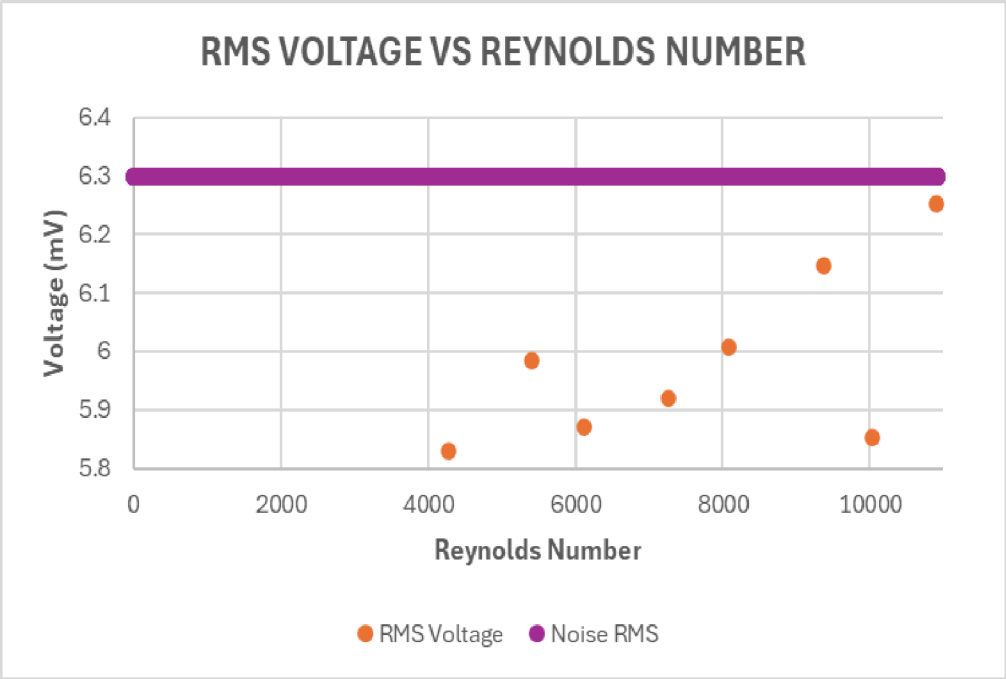

Figure 19 Variations of RMS Voltage with the Reynolds Number High-Speed Mode

5. Discussion

The primary objective of this study was to investigate the energy harvesting potential of a piezoelectric cylinder subjected to airflow-induced vibrations. This section critically analyses the experimental findings, drawing insights from the air speed measurements, valve settings, and piezoelectric voltage results to understand the efficacy and practical implications of the energy harvesting setup.

Air speed Measurement and Flow Characteristics

The determination of the necessary sampling time (3.1) revealed that a 50-second averaging period was optimal for obtaining stable and reliable airflow measurements. This finding is crucial for ensuring consistent data quality across all experiments. The determination of the speed profile at various locations in (3.2) identified that positioning the piezoelectric cylinder 8 cm from the outlet of the axial ventilator resulted in the most uniform airflow. This uniformity is vital for maximising the vibrational response of the piezoelectric cylinder and, consequently, its energy harvesting efficiency.

Effect of Valve Settings on Air speed

The measurement of air speed at various valve settings in (3.3) demonstrated that both low-speed and high-speed modes of the axial ventilator exhibited the highest air speeds around k = 4. This consistency in optimal valve settings across different operational modes suggests a robust configuration for maximising airflow, conducive to energy harvesting. The analysis also highlighted the importance of understanding the flow dynamics at different valve settings to optimise the positioning and configuration of the piezoelectric cylinder for maximum energy capture.

Piezoelectric Voltage Response

The piezoelectric voltage measurements in both low-speed and high-speed modes indicated a clear relationship between airflow speed, valve settings, and the generated RMS voltage. The data showed that higher air speeds correlated with increased RMS voltage outputs from the piezoelectric cylinder. This relationship in the specified valve setting range underscores the

potential for precise tuning of the system to maximise energy harvesting efficiency. Moreover, the Reynolds number analysis provided insights into the flow regime's impact on piezoelectric performance, with higher Reynolds numbers corresponding to more significant voltage generation.

Practical Implications and Optimisation

The experimental results suggest several practical implications for designing and implementing piezoelectric energy harvesting systems in real-world applications. Firstly, ensuring uniform airflow and stable measurement conditions is essential for reliable performance. The identification of optimal valve settings (k values 4 to 8) for both low-speed and high-speed modes provides a guideline for configuring similar systems. Additionally, since the RMS voltage fluctuates less at higher speeds, operating at these speeds could help define the speed-voltage relationship more accurately.

6. Conclusions

This study has successfully demonstrated the potential of a piezoelectric cylinder for energy harvesting from flow-induced vibrations. The key conclusions drawn from the experiments are as follows:

Optimal Positioning and Sampling Time: Positioning the piezoelectric cylinder 8 cm from the outlet of the axial ventilator ensures uniform airflow, which is critical for consistent vibration and energy harvesting. The 50-second averaging period for airflow measurements provides stable and reliable data, essential for accurate analysis and optimisation.

Valve Settings and Airflow Optimisation: The experimental data indicated that valve settings corresponding to k values between 4 and 8 provide the optimal airflow for energy harvesting. This range yielded a linear increase in air speed and voltage, with higher speeds resulting in more consistent and higher voltage outputs. The findings suggest that proper valve adjustment is crucial for maximising the efficiency of piezoelectric energy harvesters.

Increase of Voltage with Increased Speed: The study found that as the airflow speed increased, the generated voltage also increased, demonstrating a clear and predictable relationship. Higher speeds led to less fluctuation in voltage, indicating a more stable and efficient energy conversion process at these conditions.

Design Considerations for Practical Applications: For practical implementations, ensuring uniform airflow, stable measurement conditions, and optimal speed settings are crucial to the system's energy harvesting performance. These factors are essential for designing efficient and effective piezoelectric energy harvesting systems.

Future Work

Future research should explore the use of different piezoelectric materials, varying geometries, and alternative flow configurations to further enhance the energy harvesting capabilities. Integrating advanced data acquisition techniques and real-time optimisation algorithms could provide deeper insights into the dynamic behaviour of piezoelectric energy harvesters and their potential applications across various industries. Additionally, exploring the scalability of these systems and their integration into existing energy infrastructure could pave the way for practical and sustainable energy solutions.

7. References

[1] Jain, Toshit, B D Y Sunil, Mustafa Asaad Hasan, Alok Jain, Swathi B, and Neeraj Chahuan. "Smart Materials for Sensing and Actuation: State-of-the-Art and Prospects." Edited by V. Msomi and T. Ngonda. E3S Web of Conferences 505 (2024): 01034. https://doi.org/10.1051/e3sconf/202450501034.

[2] Otsuka, K., & Wayman, C. M. (1998). Shape Memory Materials. Cambridge University Press.

[3] Behera, Ajit. "Piezoelectric Materials." In Advanced Materials, by Ajit Behera, 43–76. Cham: Springer International Publishing, 2022. https://doi.org/10.1007/978-3-030-80359-9_2.

[4] Bar-cohen, Yoseph. "Electroactive Polymers as Artificial Muscles - Reality and Challenges." In 19th AIAA Applied Aerodynamics Conference. Anaheim,CA,U.S.A.: American Institute of Aeronautics and Astronautics, 2001. https://doi.org/10.2514/6.2001-1492.

[5] Asdrubali, Francesco, and Umberto Desideri, eds. "Chapter 6 - Building Envelope." In Handbook of Energy Efficiency in Buildings, 295–439. Butterworth-Heinemann, 2019. https://doi.org/10.1016/B978-0-12-812817-6.00039-5.

Harvesting in a Random Flow Field."

[6] Sarviha, Amir, and Ebrahim Barati. "Piezoelectric Energy Harvester for Scavenging Steady Internal Flow Energy: A Numerical Investigation." Journal of the Brazilian Society of Mechanical Sciences and Engineering 45, no. 8 (August 2023): 398. https://doi.org/10.1007/s40430-023-04338-z

[7] Teimourian, Amir, and Hanifa Teimourian. "Vortex Shedding Suppression: A Review on Modified Bluff Bodies." Eng 2, no. 3 (July 27, 2021): 325–39. https://doi.org/10.3390/eng2030021.

[8] Mendoza, M., H. J. Herrmann, and S. Succi. "Preturbulent Regimes in Graphene Flow." Physical Review Letters 106, no. 15 (April 14, 2011): 156601. https://doi.org/10.1103/PhysRevLett.106.156601.

[9] Xu, Xinyong, Suiqi Chen, Xiangyang Meng, and Li Jiang. "Characteristics and Hazards Analysis of Vortex Shedding at the Inverted Siphon Outlet." Sustainability 14, no. 22 (November 9, 2022): 14744. https://doi.org/10.3390/su142214744.

[10] Khalak, A, and C.H.K Williamson. “MOTIONS, FORCES AND MODE TRANSITIONS IN VORTEX-INDUCED VIBRATIONS AT LOW MASS-DAMPING.” Journal of Fluids and Structures 13, no. 7–8 (October 1999): 813–51.

[11] Liu, Yunqing, Thomas A. N. Berger, Biao Huang, Qin Wu, and Mohamed Farhat. “Vortex Shedding from a Composite Hydrofoil: Experimental Evidence of a Novel ‘Partial Lock-In.’” Physics of Fluids 35, no. 12 (December 14, 2023): 125132. https://doi.org/10.1063/5.0184582.

[12] Strykowski, P. J., and K. R. Sreenivasan. “On the Formation and Suppression of Vortex ‘Shedding’ at Low Reynolds Numbers.” Journal of Fluid Mechanics 218 (1990): 71–107. https://doi.org/10.1017/S0022112090000933.

[13] Noor, Nazihah Binti Mohd. “ANALYSIS OF VORTEX SHEDDING IN VARIOUS BODY SHAPES,” n.d.

[14] Schlichting, Hermann, and Klaus Gersten. Boundary-Layer Theory. Berlin, Heidelberg: Springer Berlin Heidelberg, 2017. https://doi.org/10.1007/978-3-662-52919-5.

[15] " Take Vortex Shedding Seriously," [Online]. Available: https://www.mecaenterprises.com/take-vortex-shedding-seriously/. [Accessed May 2024].

[16] Kumar, Anuj, Nidhil M.A. Rehman, Pritam Giri, and Ratnesh K. Shukla. “An Asymptotic Theory for the High-Reynolds-Number Flow Past a Shear-Free Circular Cylinder.” Journal of Fluid Mechanics 920 (August 10, 2021): A44. https://doi.org/10.1017/jfm.2021.446.

[17] Williamson, C. H. K. (1996). "Vortex Dynamics in the Cylinder Wake." Annual Review of Fluid Mechanics, 28(1), 477-539.

[18] Hover, F. S., A. H. Techet, and M. S. Triantafyllou. “Forces on Oscillating Uniform and Tapered Cylinders in Cross Flow.” Journal of Fluid Mechanics 363 (May 25, 1998): 97–114. https://doi.org/10.1017/S0022112098001074.

[19] Zdravkovich, M. M. (1997). Flow around Circular Cylinders Volume 1: Fundamentals. Oxford Science Publications.

[20] Khan, Umair, William Pao, and Nabihah Sallih. “A Review: Factors Affecting Internal Two-Phase Flow-Induced Vibrations.” Applied Sciences 12, no. 17 (August 23, 2022): 8406. https://doi.org/10.3390/app12178406.

[21] Jaiman, Rajeev, Guojun Li, and Amir Chizfahm. Mechanics of Flow-Induced Vibration: Physical Modeling and Control Strategies, 2023. https://doi.org/10.1007/978-981-19-8578-2.

[22] U.S. Department of Energy. DOE HANDBOOK, DESIGN CONSIDERATIONS.

[23] " Analysis of Wind-Induced Vibrations on HVTL Conductors Using Wireless Sensors," [Online]. Available: https://www.mdpi.com/1424-8220/22/21/8165. [Accessed May 2024].

[24] " Aeroelasticity & Flutter - Comprehensive Aeroelastic Analysis and Test Solutions," [Online]. Available: h https://www.ata-e.com/services/analysis/aeroelasticity-flutter/. [Accessed May 2024].

[25] "5 Niche Energy Harvesting Technologies." (Online) Available at: https://www.onio.com/article/niche-energy-harvesting-technologies.html. Accessed on 6th April 2024.

[26] Nishi, Y., Ueno, Y., & Miyamoto, T. (Department of Systems Design for Ocean-Space, Yokohama National University, Yokohama, Kanagawa, Japan). "Energy Harvesting Using Wake-Induced Vibration: Experiment in Circulating Water Channel."

[27] Wang, D-A, and H-H Ko. “Piezoelectric Energy Harvesting from Flow-Induced Vibration.” Journal of Micromechanics and Microengineering 20, no. 2 (February 1, 2010): 025019. https://doi.org/10.1088/0960-1317/20/2/025019.

[28] Adhikari, Rastogi, and Bhattacharya, “Piezoelectric Vortex Induced Vibration Energy Harvesting in a Random Flow Field.”

[29] "Properties of PZT-5A Piezoelectric Material," [Online]. Available: https://info.piezo.com/hubfs/Data-Sheets/piezo-PZT-5A_PZT-5H-material-properties.pdf/. [Accessed May 2024].

[30] N V V, Krishna Chaitanya, and Dipankar Chatterjee. “Effect of Blockage on Fluid Flow Past a Square Cylinder at Low Reynolds Numbers.” Sādhanā 47, no. 1 (March 2022): 4. https://doi.org/10.1007/s12046-021-01777-z.